UNIVERSITAT POLITÈCNICA DE VALÈNCIA

ESCUELA TÉCNICA SUPERIOR INGENIEROS INDUSTRIALES VALENCIA

TRABAJO FIN DE MASTER EN INGENIERÍA BIOMÉDICA

NANOMECHANICAL ANALYSIS OF CELL MEMBRANE MODELS USING ULTRA HIGH FREQUENCY ACOUSTIC SURFACE SENSORS

AUTHOR: Carlos Guerrero Calatayud

SUPERVISOR: Ilya Reviakine

SUPERVISOR: Gloria Gallego Ferrer

Academic year: 2017-18

Acknowledgements

Gracias al profesor Jesus Salgado del Membrane Biophysics Group, Instituto de Ciencia Molecular (ICMol), Univ. de València por permitirnos utilizar sus instalaciones para la preparación de los liposomas.

Gracias a mi hermana, Celia, que a pesar de estar estudiando el MIR sacaba veinte minutos para corregir mi inglés. Siempre con sorna.

Gracias a mis tutores, Gloria Gallego Ferrer y, especialmente, a Ilya Reviakine. Decía Bernardo de Chartres que somos como enanos aupados a hombros de gigantes. No somos capaces de ver cosas lejanas por nuestra agudeza visual, sino por la altura que nos prestan.

No podría haber trabajado con gigantes más altos.

General Index

ABSTRACT

Quartz crystal microbalance (QCM) is a sensing technique that uses the piezoelectric effect of quartz crystals to produce shear acoustic waves. Thanks to their rapid decay, they concentrate all their energy near the surface of the crystal, making QCMs surface-specific. It stands out due to its capability of sensing analyte amounts as well as properties in liquid media non-destructively and the possibility of coating the crystal surface with bioreceptors, turning QCM devices into highly specific biosensors capable of detecting small amounts of the desired analytes in liquids. Advanced QCMs measure two variables: frequency "f" and dissipation "D". To first order, frequency "f" is related to the mass of the analyte on the crystal surface and dissipation "ΔD" to the viscoelastic or geometrical properties of analyte through its ability to dissipate the energy of the shear acoustic waves in liquids.

The sensitivity of a QCM can be quantified in terms of its Sauerbrey constant, which is defined as ($C = -\frac{\Delta f}{\Delta m}$), where Δm is the mass of the adsorbed analyte, under conditions where $\Delta D \cong 0$. The Sauerbrey constant "C", depends on the properties of quartz and on the fundamental frequency of the crystal, f_0, the later determined solely by the crystal thickness. Thus, if we want more sensitive microbalances we need to use thinner quartz crystals . For decades, the use of higher fundamental frequencies was limited by the fabrication techniques that did not permit the production of stable crystals with a thickness of micrometers . However, thanks to the latest advances in photolithographic fabrication, high fundamental frequency quartz crystal microbalance (HFF-QCM) has become a reality.

HFF-QCM is a brand-new technology with a promising future, but like all advances, it comes with challenges and limitations. The smaller dimensions of the crystal increase the stress it is subjected to, which may produce more noise or instabilities. It is also unknown how the use of higher fundamental frequencies will change the measurements observed in the classical systems.

In this context, we will try to answer two questions about HFF crystals: How they behave in comparation with regular crystals when measuring a typical lipid bilayer model and what new information may be obtained from it.

For this purpose, we designed and carried out a set of experiments comparing the performance of the 100 MHz QCM with that of the classical 5 MHz one. The comparison was performed using a well-known cell membrane model that has in the past been extensively investigated by QCM. This model is based on the adsorption of phospholipid (DOPC) small unilamellar liposomes (SUVs) on a SiO$_2$coated crystal prompting a transformation from surface adsorbed liposomes to a surface-supported lipid bilayer. The transition between the liposomes and the bilayer, as well as the properties of the bilayer as a Sauerbrey film, allow a systematic comparison between the quartz crystals of the two fundamental frequencies.

For the first time, we formed a successful lipidic bilayer in an HFF crystal. The frequency sensitivity of the HFF crystals has turned to be similar to the regular ones, though the dissipation sensitivity was 5 times greater. This is specially important because signify that the lipid bilayer attenuate more the high frequency shear waves, something that had never been observed before.

Resumen

La *"Quartz crystal microbalance (QCM)"* es una técnica de sensado que utiliza el efecto piezoeléctrico de los cristales de cuarzo para producir ondas acústicas de corte que, gracias a su rápido decaimiento, concentran toda su energía cerca de la superficie del cristal, volviéndola altamente específica al medio en el que se encuentra. La QCM destaca gracias a su capacidad de captar no destructivamente las propiedades acústicas del analito en un medio líquido además de por poder recubrir la superficie del cristal con cualquier bioreceptor, convirtiendo el cristal en un biosensor altamente específico capaz de detectar pequeñas cantidades de analito en grandes cantidades de agua.

La sensibilidad puede ser cuantificada en los términos de la constante de Sauerbrey, definida como ($C = -\frac{\Delta f}{\Delta m}$), donde Δm es la masa del analito adsorbido bajo las condicione de cambio de disipación zero $\Delta D \cong 0$. La constante de Sauerbrey $"C"$ depende solamente de las propiedades del cuarzo y su frecuencia fundamental, f_0, más tarde determinada solamente por el grosor del cristal. Por lo tanto, si queremos conseguir microbalanzas más sensibles, es necesario utilizar cristales de cuarzo más finos. Durante décadas, la utilización de frecuencias fundamentales altas ha estado limitada por técnicas de fabricación incapaces de producir cristales con un grosor del orden de micrómetros. Sin embargo, gracias a las nuevas técnicas de fabricación fotolitográfica, las microbalanzas de cristal de cuarzo de alta frecuencia (HFF-QCM) se han vuelto una realidad.

Actualmente, la HFF-QCM es una novedosa tecnología con un futuro prometedor, pero al igual que todos los avances, existen retos y limitaciones. El tamaño reducido del cristal incrementa el estrés al que está sometido, lo cual puede producir un mayor nivel de ruido e inestabilidades. También nos es desconocido como el uso de frecuencias fundamentales más altas puede cambiar las medidas tomadas de los sistemas clásicos.

En este contexto, se ha diseñado y realizado un proceso experimental para comparar el desempeño de un cristal HFF de 100 MHz con un cristal de 5 MHz. La comparación se ha realizado usando un conocido modelo de membrana celular que ha sido extensivamente estudiado con QCM. Este modelo se basa en la adsorción de pequeños liposomas fosfolípídicos (DOPC) unilamelares (SUVs) en un cristal con una cobertura de SiO_2. Esta cobertura provocará la rotura de los liposomas pasando de una capa de liposomas adsorbidos a una bicapa lipídica. La transición entre los liposomas y la bicapa, y a su vez las propiedades de la bicapa como una "capa Sauerbrey", permiten la comparación de los dos cristales de cuarzo con frecuencias fundamentales diferentes.

Por primera vez, hemos formado una bicapa lipídica en la superficie de un cristal HFF. La sensibilidad en frecuencia de los cristales HFF ha resultado ser parecida a la de los cristales normales, sin embargo, la sensibilidad en disipación es 5 veces mayor. Este último hecho es de vital importancia, pues significa que la bicapa lipídica atenúa más las ondas de corte de alta frecuencia, cosa que nunca hasta ahora se había observado.

Resum

La "Quartz Crystal microbalance (QCM)" és una tècnica de detecció, mesura i transmissió que utilitza l'efecte piezoelèctric dels cristalls de quars per produir ones acústiques de tall que, gràcies a la seua ràpida dissipació, concentren totes les seues energies prop de la superfície del cristall, tornant-la altament específica al medi on es troba. La QCM destaca gràcies a la seua capacitat de sensar no destructivament les propietats acústiques de l'anàlit en un medi líquid i per recobrir la superfície de cristal amb qualsevol bioreceptor, convertint el cristall en un biosensor altament específic capaç de detectar xicotetes quantitats d'anàlit de grans quantitats d'aigua.

Els dispositius QCM moderns mesuren dos variables: el canvi en freqüència "Δf" i en dissipació "ΔD". Δf està relacionat amb la massa dipositada en la superfície del cristall i ΔD es relaciona amb les propietats viscoelàstiques de les microestructures sensades en la superfície del cristall, així com la seua capacitat de dissipar l'energia de les ones acústiques de tall. El canvi en freqüència "Δf" és proporcional al canvi de masses en la superfície del cristall quan aquesta massa forma una pel·lícula elàstica (ΔD = 0) i homogènia. Amb aquestes condicions, l'equació de Sauerbrey s'acomplirà ($\Delta f = -\frac{1}{C} m_f$). La constant de Sauerbrey "C", depén solament de les propietats del quars i la seua freqüència fonamental "f_0", regida exclusivament pel grossor del cristall. En aquest sentit, si fabriquem QCM amb una major sensibilitat, és necessari usar cristalls més prims per aconseguir una major freqüència fonamental. Durant dècades, la utilització de freqüències fonamentals altes ha estat limitada per tècniques de fabricació incapaces de produir cristalls amb un grossor de l'ordre de micròmetres. No obstant això, gràcies a les noves tècniques de fabricació fotolitogràfica i els dissenys en MESA, les microbalances de cristall de quars d'alta freqüència (HFF-QCM) han esdevingut una realitat. Nogensmenys, les implicacions d'utilitzar cristalls d'alta freqüència no solament es limiten a un augment en la sensibilitat. Les denominades "noves físiques", l'augment en soroll, l'àrea sensada etc. Són factors que caldria tindre en compte.

Actualment, la HFF-QCM és una novedosa tecnologia amb un futur prometedor, encara que l'evidència experimental en el tema és limitada. La comunitat científica i tecnològica requereixen proves de funcionament comparat amb la tecnologia QCM normal i exemples de noves aplicacions per a la HFF-QCM.

En aquest context, s'ha dissenyat i realitzat un procés experimental per comparar el desempenyorament d'un cristall HFF de 100 MHz amb un cristall de 5 MHz sota les condicions d'aplicació de l'equació de Sauerbrey (ΔD = 0). Per acomplir aquestes condicions s'ha utilitzat un conegut model de membrana cel·lular. El model consisteix en l'absorció de xicotets liposomes unilaminars (SUV) en un cristall recobert per SiO_2. Els liposomes seran absorbits per la superfície, creant una capa vesicular de superfície. Esta capa es trencarà eventualment a causa de les forces hidròfiles produïdes pel recobriment de SiO_2. La transició de liposoma a bicapa permet assegurar que l'equació de Sauerbrey s'acompleix, doncs el sistema passa de ser viscoelàstic $\Delta D \neq 0$ a ser elàstic ΔD = 0 (bicapa).

DOCUMENT 1:
Report

Report Index

Objectives

In the latest years, the improvement in fabrication technology has permitted the invention of smaller and more sensitive quartz crystals, named High Fundamental Frequency Crystals (HFF-QCM). However, the differences between classical crystals and HFF crystals are not limited only to the reduction in size and the subsequent increase in sensitivity. Other considerations such as wave penetration, noise generation or new physics considerations.

At this point, two questions should be answered about HFF crystals: What is its performance in comparation with regular crystals when measuring a standard model that follows the Sauerbrey relation? And: What new information can gather these new HFF crystals from this standard model?

The Sauerbrey relation ($\Delta f = -\frac{1}{c} m_f$) is the most known equation for QCM. The mass above the crystal "$m_{f"}$" is proportional to the frequency changes Δf. However, this relation is only valid when the mass above the crystal form a thin, homogenic and rigid film. Historically the most extended model to accomplish these conditions is the phospholipid bilayer. The phospholipidic bilayer is a cell membrane model, so is especially interesting analyze what new information can be obtained with HFF crystals.

The objective of this Thesis is to compare and analyze the performance of a high fundamental frequency crystal of 100 MHz against a normal crystal of 5 MHz in QCM technique evaluating the absorption of DOPC unilammellar liposomes with a diameter of $60\ nm$ and its transition to phospholipidic bilayer simulating a cell membrane with the additional objective of provide new information about their nanomechanical and physico-chemical properties.

The compare and analyze objective can be detailed as:

- Compare the stability and sensitivity of a 100 MHz crystal (HFF) and a 5 MHz crystal in a continuous viscous media. (before liposomes injection)

- Study and compare the absorption forces of liposomes with the surface of a 100 MHz crystal (HFF) and a 5 MHz crystal.

- Study the liposome transition to bilayer with a 100 MHz crystal (HFF) and a 5 MHz crystal.

- Study the acoustic properties of the different phospholipidic structures in contact with a 100 MHz crystal (HFF) and a 5 MHz crystal. (bilayer, liposomes…)

Motivation

The realization of this work was motivated for my interest to make an external internship in a bioengineering company. In this context, AW Sensors represents exactly the characteristics of the biomedical engineer: multidisciplinary, creative, innovative, in constant contact with the market and with the capacity to learn and reinvent themselves.

Focusing in QCM technology, it is exciting the quantity of multidisciplinary knowledge involved (instrumentation, physics, biochemistry etc.) Moreover, the potential it has to become a reliable multipurpose biosensor.

Since the beginning of my degree I wanted be a part of the process that transforms basic research into useful products for the community. Working in the development of new applications for high frequency crystals in QCM has given me the privilege of participating in this process and contribute with my effort. Most of all, it has allowed me to learn things that are hardly teachable in class. The work dynamic in a lab, the importance of supporting our colleagues and being supported by them, the capability of using all the tools at your reach, the importance of learning English in a working environment etc. This Thesis was a personal challenge in view of working outside the comfort zone that supposes the university in addition to facing a new perspective which I didn't know if I was prepared for. The main motivation in conducting this Thesis is the certainty of becoming a better professional at its end.

Introduction

1. BIOSENSORS

Measuring biological or chemical reactions is a fundamental part of many technologies that have evolved over the last decades. A sensor is a device which detects or measures a chemical property and records, indicates, or otherwise responds to it. For example, the Clark electrode is a sensor that measures oxygen concentration by monitoring the current at the Pt electrode as it is reduced by the oxygen. The need to identify and quantify increasingly complex analytes resulted in the invention of biosensors. The difference between sensors and biosensors is the utilization of biological entities[1] as a part of the sensing process [2]. That brings to the biosensors a new dimension of measuring thanks the affinity and specificity of the biological interactions and promises greater miniaturization.

Examples of biological interactions and biological entities used in biosensors include antibody-antigen interactions[3], the enzymatic reactions [4], nucleic acid probes [5] or even whole cells[6].

The first true biosensor was the result of combining the "Clark electrode" with a film of immobilized glucose oxidase[7]. Glucose will interact with glucose oxidase and liberate an equivalent quantity of oxygen into the Clark electrode, which would then produce a proportional increase in the potential related to the concentration of glucose. Some of the best-known biosensors are the pregnancy tests, the glucose meters, or the human papilloma virus HPV test and can be used in food safety, drug discovery, disease diagnostics, environmental monitoring etc.

Other components of biosensors include transducers that transform biological or chemical reactions such as antibody-antigen interactions into interpretable signals. Some examples of transducers are piezoelectric crystals, electrochemical electrodes or solvatochromic fluorophores. Finally, the signal of the transducer is registered by an electronic detection system (or equivalent), amplified, processed, and displayed or used in a closed-loop control circuit to control a response.

This Thesis is concerned with the development and investigation of a particular class of transducers used in sensing and biosensing systems, namely quartz crystal microbalances (QCM) that are based on shear mode piezoelectric crystals. A schematic view of a biosensor based on the QCM sensing technique is described in **figure 1**.

Since the operation of QCM is based on the principle of piezoelectricity, relevant concepts are introduced next.
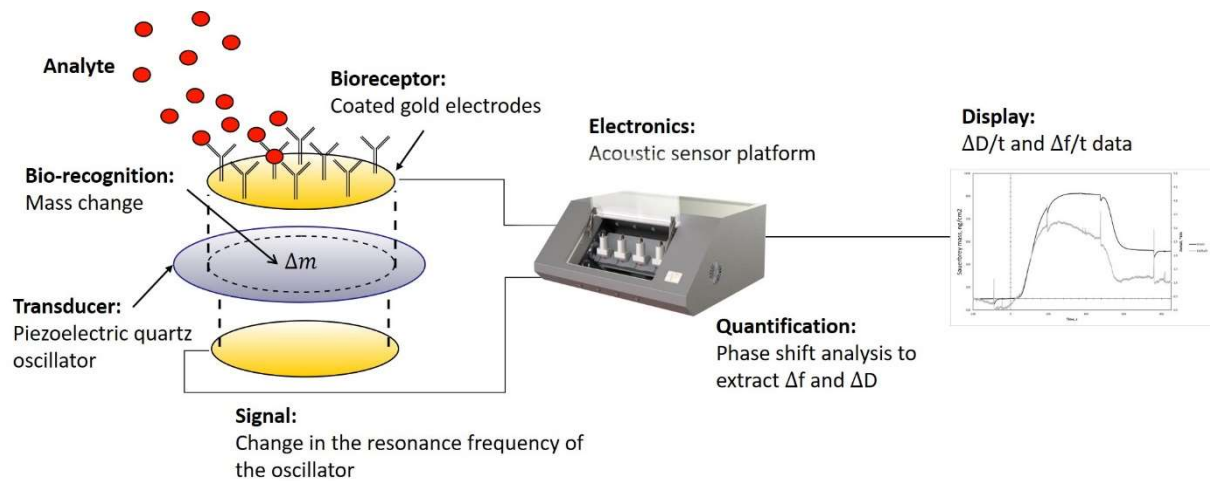
Figure 1: *A schematic of a QCM-based biosensor.*
The active part of a biosensor is the biological entity, in this case an antibody, that interacts with the analyte of interest. In QCM, which is based on a gold-coated quartz oscillator, the antibody is typically applied to the gold electrode. Analyte binding to the antibody is detected as a change in the oscillating frequency of the piezoelectric quartz crystal that acts as a transducer. The frequency shift is precisely measured by the electronics of the QCM through phase-shift analysis described in more detail in the main text. The information is displayed as a variation of frequency Δf in time. Advanced QCMs also measure a quantity called dissipation ΔD that describes energy losses in the film (see main text for further explanation).

2. BRIEF INTRODUCTION TO PIEZOELECTRICIY AND SHEAR ACOUSTIC SENSORS

The piezoelectric effect is described as the mechanical deformation of a piezoelectric crystal under the influence of an electric field. When the electric field applied to the crystal is alternating with the frequency matching the eigenfrequency of the piezoelectric crystal, the deformation becomes cyclical, creating a mechanical wave. The type of mechanical wave produced will be longitudinal or transverse (normal sound or shear sound). That will be determined by the symmetry of the crystal. Longitudinal waves create an alternating pressure pattern in the media. Shear waves are a secondary transverse waves that create periodical shear stress oscillations in the media due to the antiparallel horizontal movement that is transmitted to the media.

A significant difference between the two types of waves is the decay length. While the pressure nature of the longitudinal waves permits them to travel large distances in viscous and compressible fluids unperturbed, the shear waves decay rapidly. For the longitudinal waves the decay length is in the order of meters but for transverse waves, the decay length is of the order of the wavelength. In practice, it will be of the order of a few nm. Due to the rapid decay, the shear waves concentrate all their energy near the surface, which makes them surface-specific.[8] They are able to distinguish really small changes in the organization of the media in contact with the surface. This makes shear-based crystals useful in sensing and biosensing applications.

The most common example of a shear-acoustic sensing device is QCM. It is based on an AT-cut quartz crystal that serves as a as a shear acoustic crystal (Figure 2).
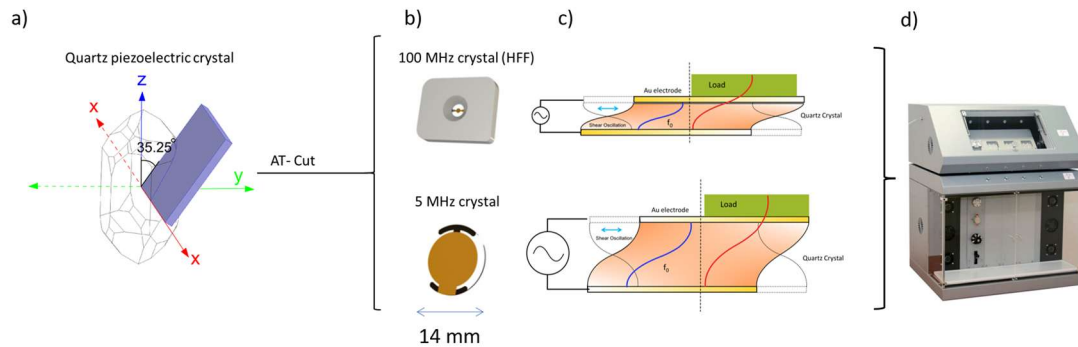
Figure 2: *QCM basics*

(a) A crystal of quartz, with the crystallographic axes indicated. Thickness-shear mode (TSM) crystals are made by cutting thin plates of quartz at an angle of 35° 25' to the Z-axis (blue rectangle); the so-called AT-cut.

(b) A 100 MHz (top) and a 5 MHz (bottom) TSM crystals. The 100 MHz crystal is mounted on a polymeric support (beige), while the 5 MHz crystal is unmounted. Gold electrodes are evaporated over the quartz to apply the voltage that drives the oscillations.

(c) Schematic illustration of the thickness-shear mode vibrations in the unloaded and the loaded crystals. The wavelength of shear sound is given by the thickness of the quartz plate, ~ 300 um for the 5 MHz and ~ 30 um for the 100 MHz crystal. Applying the load increases the wavelength and correspondingly decreases the frequency of the oscillations.

(d) An AWSensors QCMD instrument with a fluidics module (bottom) and the sensing electronics box (top).

.

3. WHAT IS QCM?

QCM, or QCMD as it is more often called today (Figure 2), is a sensing technique. It works as such because the resonance frequency of the shear acoustic crystal depends on its environment and changes if the crystal is immersed in liquid or if a thin film of material is deposed on top of the crystal as shown in Figure 2B. QCM measures the changes in the resonance frequency. It is described as a "microbalance" because of a linear relationship between the resonance frequency change and the mass of the deposited layer. The principle is schematically illustrated in Figure 2B. The resonance frequency, f_n, is determined by the crystal thickness d:

$$f_n = \frac{nc}{2d}$$

where *c* is the speed of shear sound in quartz and *n* is the over tone order. Factor of 2 originates from the fact that the opposite faces of the quartz crystal are located at the antinodes of the shear wave and have to move in the opposite directions. For the same reason, *n* is odd. The first of the resonance frequencies $n = 1$ is called the fundamental frequency (f_0) and the following ones (n= 3,5,7...) are called overtones(f_3, f_5, f_7 ...).

As we can see, the resonance frequency of the crystal only depends on the physical properties of the quartz (density and shear modulus) and the thickness of the crystal. The shear modulus of quartz and the density of quartz are constant and known:

$$\sqrt{\rho_q G_q} = 8.84 * 10^6 \frac{kg}{sm^2}$$

If the thickness of the quartz crystal increases due to the deposition of a film, as shown in Figure 2B (c.f. the blue and the red waves for the unloaded and the loaded crystals, respectively), the frequency will decrease. For thin elastic films, the decrease will be proportional to the mass of the film.

$$\Delta f_n = -\frac{n}{C} m_f = -\frac{n}{C} \rho_f d_f$$

This equation is due to Gunter Sauerbrey[9] and the constant, C, bears his name. It is defined as

i

$$C = -\frac{\sqrt{\rho_q G_q}}{2 f_0^2}$$

The surface of the quartz crystal can be coated with diverse substances. If it's covered with a bioreceptor such as an antibody (Figure 1) and measures the mass of the adsorbed antigen, QCM becomes a biosensor.

4. SENSITIVITY OF A QCM SENSOR

The sensitivity of the sensor will be equal to the inverse of Sauerbrey constant "C":

$$Sensitivity = \frac{1}{C} = \frac{n * 2 f_0^2}{\sqrt{\rho_q d_q}}$$

From this equation, it is clear that the sensitivity depends on the fundamental frequency, and higher frequencies are expected to achieve higher sensitivities.

For a crystal of 100MHz, the Sauerbrey sensitivity is:

$$C_{100} = \frac{8.84 * 10^6}{2 * (100 * 10^6)^2} = 0.04 \frac{ng}{cm^2 Hz}$$

For the crystal of 5MHz, the Sauerbrey sensitivity is:

$$C_5 = \frac{8.84 * 10^6}{2 * (5 * 10^6)^2} = 18 \frac{ng}{cm^2 Hz}$$

This improvement in sensitivity is what drives the research into high-frequency crystals, called HFF-QCM that uses crystals with $f_0 > 40\ MHz$. This is the reason why HFF QCM was chosen as the basis of the work presented in this Thesis.
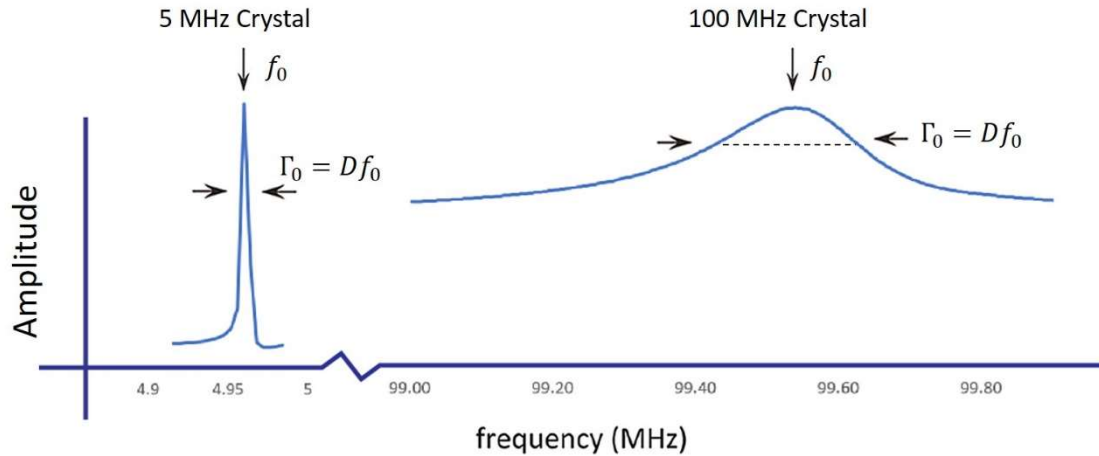
Figure 3: Resonances observed with a 5 MHz crystal and 100 MHz crystal is in air. The excitation frequency is plotted on the x-axis. The y-axis represents the current passing through the crystal or its mechanical equivalent, the amplitude of the crystal's shear motion. For the 5 MHz and 100MHz crystals, the quality factors in water are respectively $Q_5 = 7590$ and $Q_{100} = 357$.

5. NOISE IN QCM EXPERIMENTS

The Sauerbrey constant shows only one side of the sensitivity problem. On the other hand, sensitivity of a quartz crystal is limited by noise. One source of noise is the crystal itself. To understand why that is the case, it is necessary study energy dissipation D associated with the oscillations. The dissipation is defined in figure 3, where the resonance peaks for the 5 MHz crystal and the 100 MHz crystal are shown.

Energy dissipation is the normalized value of bandwidth of the signal (Γ).

$$D = 1/Q = \frac{2\Gamma}{f_0}$$

Quality factor Q is the inverse of the dissipation and is the ratio of energy stored by to the energy lost in the crystal per oscillation cycle.

As is shown, the 100 MHz crystal is less efficient: it dissipates more energy (has a broader resonance peak and a smaller quality factor) leading to a greater uncertainty in the measurement of the fundamental frequency f_0. This uncertainty will have as consequence an increase in the noise of the measurement and a corresponding decrease in sensitivity. For quartz crystals, a fundamental relationship exists between the maximum achievable quality factor and the fundamental frequency[10]:

$$Q_{max}f_0 = 1.6 * 10^{13} Hz$$

This sets the limit on the maximum attainable sensitivity of a quartz crystal. Factors of a fundamental nature that contribute to the energy losses and the consequent broadening of the resonance peak include Johnson noise and the phonon scattering noise. In practice, further limitations arise from the stress relief and accumulation between the quartz crystal and the electrodes[11], the scattering of the acoustic waves off of the surface roughness[12] etc. that broaden the resonance beyond the maximal theoretical limit, as will be shown in the Results section of this Thesis.
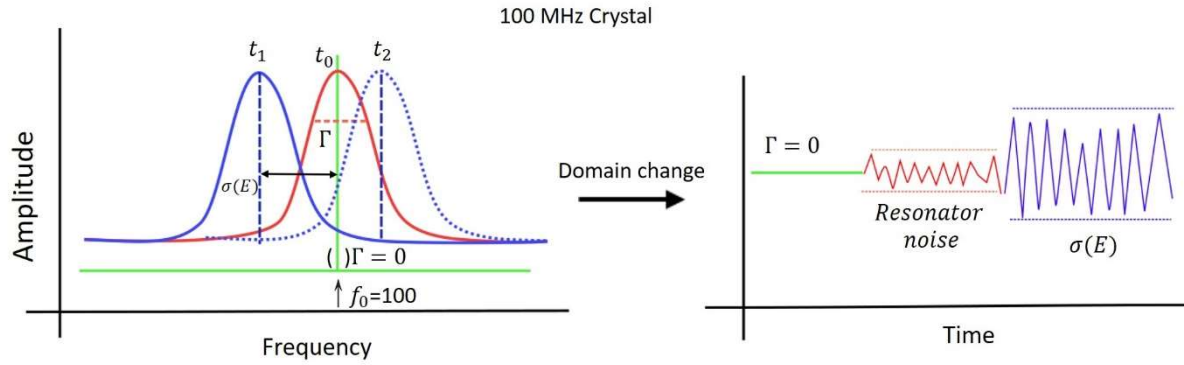
Figure 4: sources of noise. the sensitivity can be studied in the frequency domain (left) or the time domain (right). When $\Gamma = D = 0$ (no noise presence) the sensitivity will be the inverse of the Sauerbrey constant C^{-1}. However, noise will always be present. The red line shows the noise produced by the crystal (in form of an increased bandwidth). The blue line the measurements performed in the following instant, t_1, and at bit later, t_2. The phase instabilities induce a time-dependent error, $\sigma(E)$, leading to the variation in frequency with time.

Other factors contributing to the noise in the QCM measurements originate outside of the crystal. This type of noise is represented with blue in figure 4 and is called "phase stability". The phase stability is the fundamental frequency variation of successive measurements in time. It includes changes in external load, fluctuations in the ambient temperature, mounting stress, and the noise in the electronic system used to interrogate the crystal (readout methods). An important aspect of biosensor design amounts to minimizing these external sources of noise through various optimization strategies which are beyond the scope of this Thesis.

The nature of the noise produced will be determined by the way that the measure is performed. In the following we will describe the most important readout methods.

6. Means of measuring resonance frequency and dissipation

The readout methods are techniques that are used to measure the frequency f and bandwidth Γ values in QCM systems in other words, they are the methods that interrogate the crystal to obtain the final values of interest, frequency and dissipation. Figure 5 represents the most used readout methods, including the one used in this thesis, the phase shift analysis.

- o **Impedance analysis:** consists of examining the admittance of the crystal as a function of the frequency of the applied voltage. For a fixed interval of time the bandwidth is swept, and a function of the conductance is obtained. The peak of this function will determinate the resonance frequency, and the width – the bandwidth and dissipation, as shown in Figure 5 .

- o **Ring-down method:** for a fixed interval of time the driving voltage is intermittently switched off and the decay in time of the oscillation is monitored. The decay of this signal gives the information of the frequency Δf and bandwidth $\Delta \Gamma$ variations.

- o **Phase shift monitored at a constant frequency:** With this method, the quartz
  crystal is excited at a constant frequency and the phase of the electrical signal
  passing through the crystal relative to the excitation is monitored Monitoring
  the evolution of the phase at certain frequency, gives the same information that
  the impedance analysis and affords a very simple and fast electrical circuit.
  Furthermore, the cancellation of the phase instabilities potentially offers the
  possibility of a more sensitive detection[13].

All three methods provide a measure of resonance frequency and bandwidth (dissipation).
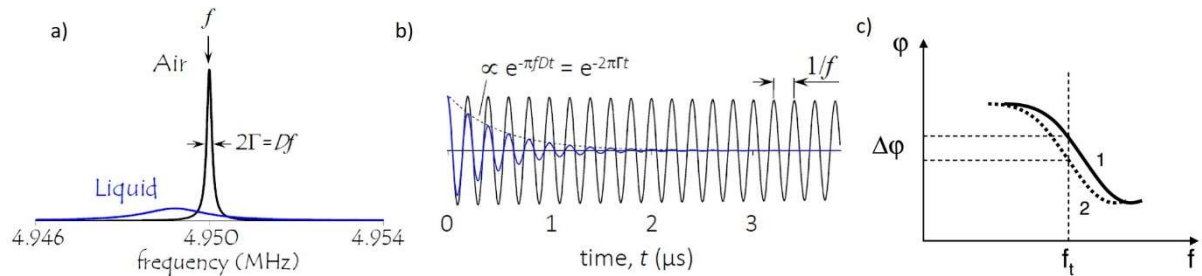
Figure 5: _readout methods_
_a) Impedance analysis realized in air (black) and water (blue). The y axis represents the current passing
through the crystal. The x axis represents the excitation frequency_
_b) Ring down method. The black line represents the measure in air and the blue represent the measure in
liquid. The driving voltage is intermittently switched off and the decay in time of the oscillation is
monitored. From the decay curve, the resonance frequency and the dissipation are extracted._
_c) Qualitative representation of the phase shift (Δφ) obtained when the crystal sensor is interrogated at
constant frequency (f t)._

7. ENERGY DISSIPATION AS A CHARACTERIZATION TOOL: MODELS FOR INTERPRETING QCMD DATA

At this point the reader may think that energy dissipation "D", is an inevitable characteristic of
the crystal that reduces de sensitivity and should be reduced at any cost. The reality is that
thanks to the mechanical behavior of the shear acoustic waves, energy not only will dissipate in
the crystal, it will dissipate in the analyte or the media. The interaction of shear waves with the
environment is ruled by the complex shear elastic modulus of the media G:

$$c = \sqrt{\frac{G}{\rho}} \qquad\qquad G = G' + iG''$$

Where c is the velocity of the shear wave, in the material and equals to the square root of the
division of the complex shear acoustic modulus G and the density of the material ρ.

G represents the way that the shear waves interact with the material. G is composed of two terms, the storage modulus G' that describes the material elasticity and the loss modulus G'' that describes viscous characteristics of the material and will be the parameter that regulate the shear acoustic energy lost in the material. If a material has a loss modulus and viscous modulus, it will show a viscoelastic behaviour.

It is possible measure the dissipation changes over time. This change will be related with the physical characteristics that affect the shear waves transmission (summarized on "G") such as density, viscosity, or even the micro-structure . Taking into consideration the dissipation changes "ΔD" in addition to the frequency changes "Δf" makes the QCM stop being just a "microbalance", a device for measuring weight of the adsorbed films, to become a sensitive tool for characterizing viscoelastic properties of the films and their organization. This explains the wide applicability of QCM in biological, chemical, and physical surface sciences, preclinical diagnostics, and other research and development fields.

Due the complexity of the interactions of the shear wave with the media, models are used to interpret QCMD data

The different types of media interacting with shear waves that are presented in this Thesis are grouped in figure 6. According to their morphology and the observed dissipation response they can be laterally homogeneous (a, b, c) or not (d). In either case, they may or may not dissipate energy (a vs b, c, d). In the following, the characteristics of these films and the approaches to data interpretation for each of them are described.
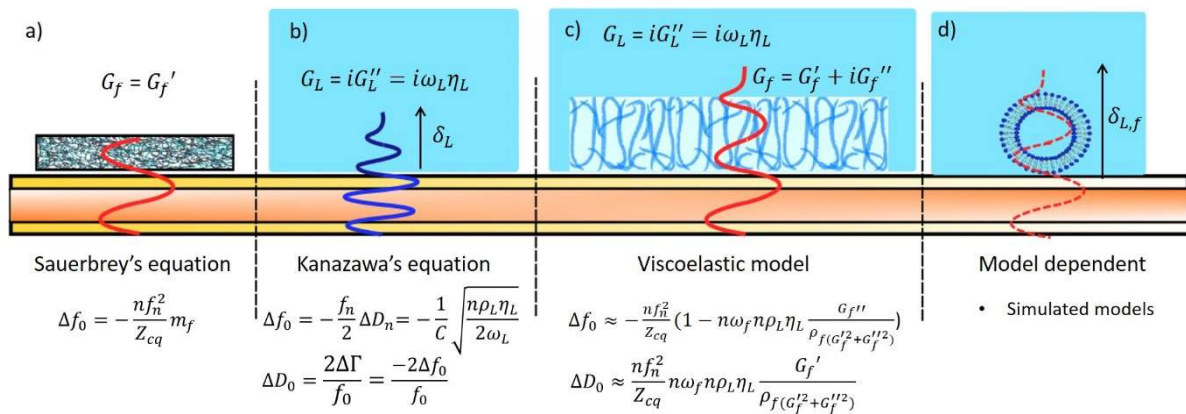
Figure 6: *Interpreting QCMD data.*

The propagation of the shear waves in the media is governed by the density rho and the shear modulus G complex of material. Three cases can be distinguished. a) For thin, stiff films, the Sauerbrey equation relates the mass of the film to the change in the resonance frequency of the sensor due to the film loading.
b) For a crystal immersed in viscous media (such as water), the Kanazawa-Gordon-Mason equation relates the frequency and dissipation shifts to the liquid density and viscosity. ($G_L = i\omega_L\eta_L$). The penetration depth δ_L determines the dissipation of the shear wave in this media
c) In the case of thin, homogeneous viscoelastic films, the frequency and dissipation shifts are related to the mass of the film attenuated by a frequency-dependent viscoelastic correction. In mixed medias, c) and d), the penetration depth $\delta_{L,f}$ is a combination of the penetration depth of both medias

d) No analytical models exist for laterally heterogeneous films such as surface-adsorbed particles or liposomes, and simulations must be used to interpret QCMD data, although in some specific cases information can be obtained from the acoustic ratio, ΔD/ΔF.

Sauerbrey relation ($\Delta f_n = -\frac{n}{C} m_f$) presupposes that the film in contact with the crystal have a behavior similar to the quartz. Thanks to the difference in thickness between the quartz crystal and the film, the shear modulus of the film can be approximated to the same value of the quartz module.

$$G_q \cong G_f$$

However, Sauerbrey relation only will be valid when the film doesn't dissipate energy, in other words, Sauerbrey model can be applied when:

$$G' \gg iG'' \quad and \quad \Delta\Gamma \ll \Delta f$$

Most of the measures performed with QCM happen in liquid media (and all of them of this Thesis). Kanazawa and Gordon, and before them, Mason, measured the viscosity of liquids with theQCM. They found that the decrease in the frequency and the increase in the dissipation were both proportional to the square root of the product of liquid viscosity and density.

$$\Delta f_0 = -\frac{f_n}{2} \Delta D_n = -\frac{1}{C}\sqrt{\frac{n\rho_L\eta_L}{2\omega_L}}$$

In the experiments where the liquid media does not change during the formation of the adsorbed film, the Kanazawa-Gordon-Mason relation is not relevant, but the realization of QCM measurements in water will have other implications discussed below.

As previously mentioned, one of the best advantages of using QCM is because is surface specific thanks to the fast decay of the shear waves in viscous fluids defined by the penetration depth:

$$\delta_L = \sqrt{\frac{\eta_L}{\pi f_0 \rho_L}}$$

The penetration depth of the shear waves in a viscous liquid δ_L is equal to the square root of the viscosity of the liquid η_L divided by pi, the fundamental frequency f_0 and the density of the liquid ρ_L.

For a 5 MHz crystal operating in water, the penetration depth will be $\delta_L = 250\ nm$.

For a 100 MHz crystal operating in water, the penetration depth will be $\delta_L = 56,43\ nm$.

The effect of the penetration depth is reducing the height of the area sensed. This combined with the smaller area of the HFF quartz crystals, cause a drastic reduction of the volume of solution sensed above the surface of the crystal, as is shown in the next figure. HFF crystals are more surface-sensitive, which can be an advantage for sensing applications.
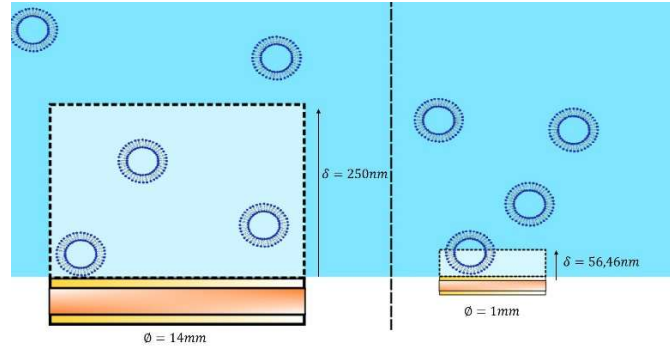
figure 7: *Concept view of the area sensed by an 5MHz crystal (left) and a 100Mhz Crystal (right)*

Finally, we must consider that some of the biological films sensed by QCM will not show an elastic behavior..

The viscoelastic model is applicable when the homogeneous film adsorbed by the quartz crystal surface have a viscoelastic behaviour, in other words its shear modulus has an imaginary component $G = G' + iG''$.

$$\Delta f_0 \approx -\frac{nf_n^2}{Z_{cq}}\left(1 - n\omega_f n\rho_L\eta_L \frac{G_f''}{\rho_{f(G_f'^2+G_f''^2)}}\right)$$

$$\Delta D_0 \approx \frac{nf_n^2}{Z_{cq}} n\omega_f n\rho_L\eta_L \frac{G_f'}{\rho_{f(G_f'^2+G_f''^2)}}$$

Viscoelastic model is hard to apply because its numerous independent variables. However, its biggest limitation is that supposes that the material absorbed is laterally homogeneous when the majority of biological particles, such as proteins, will be absorbed heterogeneously.

In that case, for sense discrete particles or nanosized objects adsorbed by the surface of the crystal such as liposomes, a particular model should be used. There is no standard to build these models because the QCM response will be governed by hydrodynamic effects and the motion of surface-absorbed particles. Some methods used are quantitative predictions limited by computational resources, bandwidth-frequency variation ratio $-\frac{\Delta\Gamma_n}{\Delta f_n}$, finite element method simulations etc.

8. THE UNIFIYING PRINCIPLE AND THE SMALL LOAD APROXIMATION

All these concepts can be unified introducing the complex frequency shift:

$$\Delta f^* = \Delta f + i\Delta\Gamma$$

Where:

$$\Delta f^* = \frac{iZ_L}{2\pi m_q} \qquad or \qquad \frac{\Delta f^*}{f_n} = \frac{iZ_L}{2\pi Z_q}$$

($m_q * f_n = Z_q = 8.8*10^6$ kg m^{-2} s^{-1})Is the areal mass density of the quartz crystal and $Z_L = Z_L' + iZ_L''$ is the load impedance, in other words, the ratio of shear stress-to-velocity at the oscillating

crystal surface. The load impedance involves all previously discussed properties of the material in relation with the shear waves. The linear relationship between the complex frequency shift and the load impedance is central to the interpretation of QCM data and is named the "small-load approximation". Thanks to this point, complex materials, such as cell cultures or vesicles can be analyzed quantitatively if the load impedance Z_L can be calculated in one way or another.

However, this linearity only is accomplished in certain circumstances:

- The frequency shift is < 1% of the fundamental frequency as is implicit in the previous equation:

$$Z_L = iZ_q \tan(\pi \frac{\Delta f}{f_n})$$

9.   NEW PHYSICS: EFFECT OF THE FUNDAMENTAL FREQUENCY ON THE ANALYTE

So far, we have commented the effect of the fundamental frequency on the measurement process (noise, sensitivity, area of observation etc.) However, depending on its acoustic characteristics and organization, the analyte will react in different ways.

Focusing on viscoelastic films, the shear modulus G is in general frequency-dependent. [14,15]. The practical interpretation of this phenomenon is that some films will show bigger viscous or elastic responses at certain frequencies. Ultimately, the behavior of a material as a function of frequency is related to the rotational and vibrational properties of the molecules making up the material, and the G(f) curves exhibit transitions between different relaxation modes. Pushing the resonance frequency and the surface sensitivity up focuses the measurement on the interactions between surfaces and lipid molecules and has the potential of revealing new physics about the molecule-surface interactions.

In the latest years, a new conception of the effect of the frequency of the shear wave on the analyte has been taken in consideration. When sensing high organized structures, at certain frequencies, the deformation caused by the shear waves will trigger a bigger reaction thanks to the resonance of this deformation. This can be used to the identification of the nanomechanical properties of the sample.

However, until now, there is no significant literature on the subject based on QCM technology.

10. HIGH FUNDAMENTAL FREQUENCY CRYSTALS

At this point the reader will have noticed that there are many theoretical implications using high fundamental frequency crystals (such as sensitivity, noise, effect on analyte, area sensed etc.) But most of the drawbacks of using HFF crystals are related with this fabrication and handling. In this section we will deepen into the high fundamental frequency crystals, its fabrication and the implications that it has into its use.

The regular crystals of 5 MHz to 10 MHz have a thickness between 0.33 mm and 0.17 mm. Such thicknesses, in combination with a diameter of approximately 14 mm, provide a sufficient mechanical stability for an easy installation in a flow cell[16]. On the other hand, HFF crystals of 100MHz have a thickness of $16\mu m$ approximately with a diameter of $1.0mm$. The measures of the 100MHz crystal used in this Thesis are represented in figure 7.
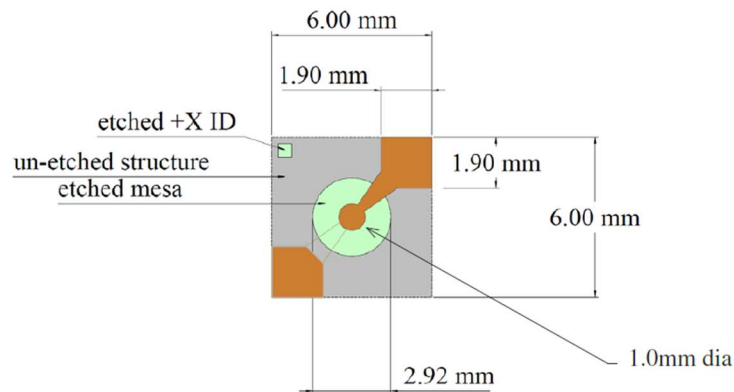
figure 8: *Scheme of AWS 100MHz crystal model.*

Ainverted mesa HFF crystal is composed of a quartz crystal where its centre has been thinned down to form a thin membrane. In the central zone gold electrodes are deposited on each of the faces of the crystal. Finally, the crystal will be mounted in a plastic support to facilitate its handling an electrical connection.

The fundamental requirements for the fabrication of HFF crystals are: small size, high quality factor and avoid or reduce as much as possible the presence of inharmonic or spurious modes in the vicinity of the fundamental mode. We will try to summarize the most important factors of the fabrication of the HFF crystals in the next points.

Spurious modes

The spurious modes are non-desired vibration movements in the crystal, in other words, are vibrations produced in non-desired directions. This vibration modes can appear due a defective cut of the quartz crystals. These modes will have his own fundamental frequency and will affect the measurement. One of the most important requirements for operating a quartz crystal as chemical sensor is the frequency stability. If the frequency separation between the harmonic and inharmonic modes is not sufficient neighbouring frequencies may cross each other. This could cause effects like mode coupling and frequency jumps. All these effects would impede a reliable frequency measurement, which serves commonly as output signal. They take special importance when speaking of HFF crystals due its reduced size. It can be avoided situating the fundamental frequency of these spurious modes in a frequency far away of the shear acoustic fundamental frequency. This can be accomplished with numerical modes [17], energy trapping methods, lapping of one or both sides of the quartz plate[18], bevelling of the quartz edges etc.

Size considerations and fabrication

For many time, the size values of HFF-QCM presented to many inconveniences in fabrication and handling [19], but thanks to the micromachining technology, which combines the photolitographic process and plasma or chemical etching techniques, the development of complicated mechanical and electrical sensor microstructures from a single substrate[20] has been possible. Specifically, new inverted mesa designs[21][17][22] have been used to overcome these issues by thinning only a small area of the sensor, while the surroundings of the device provide a supporting frame with mechanical strength.

In the process only a part of the quartz is chemically thinned down to the desired thickness in order to provide sufficient mechanical stability. The result is a thin membrane with a thick, mechanically stable outer ring. The transition zone between the thin and thick zone will be critical for the quality factor of the crystal.

However, HFF crystals still have problems due to their small size. Their low dimensions promote a mechanical instability that can be summarized in:

- Hysteresis: contamination transfer to crystals, stress relief in the electrodes etc. will cause a larger frequency change in a thinner crystal.
- Aging[23]: The aging rate tends to scale with the surface -to-volume ratio of the crystal.
- Pressure fluctuations: When HFF-QCM are taken in liquids even minute fluctuations of hydrostatic pressure can affect to the signal stability.
- Bending: due the mass of the liquid and the analyte the crystal could bend, producing incorrect measures.
- Stress: Little irregularities in the crystal surface or with the electrode contact could cause that the mass will not distributed regularly, causing stress in some zones of the crystal.

Electrode design

Electrodes, typically made of gold, are evaporated on top of the quartz for exciting the resonance. They require a minimum thickness to insure good electrical conductivity and produce the "energy trapping [24]" effect. This effect confines the thickness shear vibrations under the electrode area, improving the quality factor of the sensor. However, there is a trade-off, because thicker electrodes add more mass to the crystal and induce spurious modes. It is necessary to find a compromise solution between the thicker electrodes to improve conductivity but reduce the effects of added electrode mass and spurious modes.

11. CHARACTERIZING HIGH FUNDAMENTAL FREQUENCY CRYSTALS

The reader will have noticed that using high fundamental frequency crystals implies a lot of theoretical and technical difficulties. A systematic study of these aspects has not yet been conducted, however, the HFF-QCM has significant potential. Recent advances such as the phase shift monitored at a constant frequency readout method[25] has improved the HFF-QCM measurements in liquid. These improvements and the reduced dimensions of the crystals are leading the HFF-QCM sensors to become more miniaturized and easier to use with the objective to expand the technology from research to industrial or medical applications such as pesticide detection. Moreover, HFF QCM is the only route available currently for parallelisation (production of QCM arrays for simultaneous measurements). However, the literature on this

technology is immature. Systematic analysis of HFF sensor performance and its comparison with the classical low-frequency sensors is scarce[26],[27]. A systematic analysis with a proved and extended standard experiment is needed to provide quality information about the differences between HFF and regular crystals.

In order to guide the optimisation of the HFF crystals, an efficient means of characterizing crystal performance is required. This Thesis is therefore concerned with the investigation of such a characterization system with HFF crystals, namely, of surface-supported cell membrane models, liposomes and bilayers. In the following sections, the properties of these biological structures will be presented, and it will be shown why this system is so useful for studying the HFF QCM sensors on one hand, and conversely, what new information is to be expected from HFF analysis of this system.

12. PHOSPOLIPID STRUCTURES: LIPOSOMES AND BILAYERS

Phospholipids are a class of lipids defined for have two hydrophobic fatty acid tails joined with a glycerol molecule to a hydrophilic head containing a phosphate group. The result is a molecule with an amphipathic behavior, in other words, one part of the molecule will be hydrophobic, and the other part will be hydrophilic. The dual nature of the biomolecule will induce the creation of self-assembled structures, especially in a polar media like water. The molecule will assemble in order to minimize the contact of its hydrophobic parts with the polar media.
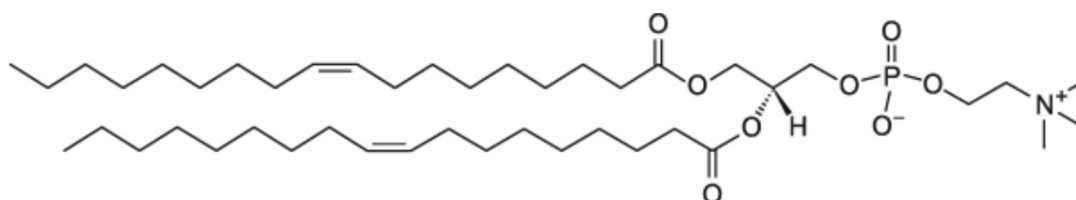
figure 9: *DOPC (1,2-dioleoyl-sn-glycero-3-phosphocholine) phospholipid. DOPC is a phospholipid that incorporate a choline as headgroup. It is possible to see in the image two fatty acid tail bonded with a glycerol molecule that has a phosphate group attached to a choline group.*

The most basic structure formed by phospholipids is the lipid bilayer. The lipid bilayer is a flat polar structure made of two layers of phospholipids. The lipid bilayer forms a really thin film compared with its lateral dimensions. At normal temperature, the bilayer will be in a fluid state. In other words, the phospholipids will have certain types of movements such as rotational, lateral or transverse. It is possible find a pure lipid bilayer when is adsorbed in a hydrophilic surface.
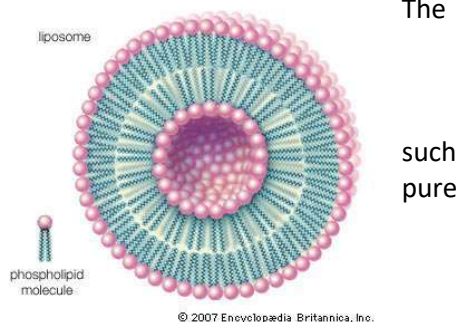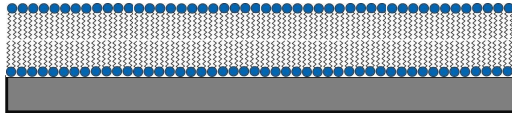
figure 11: *lipidic bilayer supported in a surface. It is composed by two sheets of phospholipids.*

figure 10: *(left) phospholipid molecule with a hydrophilic head and tow hydrophobic tails. (right) small unilamellar vesicle composed by a bilayer of phospholipids circling an inner media.*

However, the lipid bilayer will form other structures in the presence of polar dissolvent to minimize the surface in contact with it when its adhesion with the surface where it was adsorbed is not strong enough. The most common structures formed by lipid bilayers are liposomes . Liposomes are closed lipid bilayers forming a spherical particle that encircles an inner aqueous core separating it from external media.

As shown in figure 9, the liposomes can be characterized by their size and number of layers. The size of liposomes is dived in 4 categories: small, medium, large and giant as is shown in table 1.

Table 1: *Liposome clasification*

	Small	Medium	Large	Giant
Diameter (nm)	20-40	40-80	100-1000	> 1000

As their number of layers, liposomes can be described as unilamellar or multilamellar depending of the number of lipidic bilayers it is composed of.
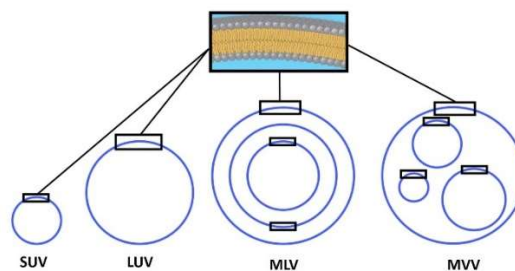
figure 12: *Types of liposomes according to their lamellarity and size. The diameter of small unilamellar vesicles (SUV) is between 20-40nm. large unilamellar liposomes (LUV) are between 100 and 1000 nm. Multilamellar vesicles (MLV) are composed of more than one bilayer and multivesicular vesicles (MVV) encapsulate other vesicles*

13. LIPOSOMES AND SUPPORTED LIPID BILAYERS AS CELL MEMBRANE MODEL

The biological membranes are basically composed by a lipid bilayer (usually forming a sphere) and proteins. The membranes play a key role in cell life. They control the transfer of information,

the transport of ions and molecules, participate in various intra- and extra- processes and act as the basic tool to separate an inner media to an external environment interacting with the rest of biological entities thanks to the proteins that are integrated in the membrane[28].

However, their study often becomes difficult due the high complexity of the cells. In the last years the use of models that simulate biological membranes has become popular[29]. These models permit the study of lipid bilayer in controlled conditions, practically, they allow the biofunctionalization of inorganic surfaces.

From small vesicles that transport and store substances to complete cells, liposomes are artificial structures that mimic one of the most important and omnipresent biological structures in nature, the membrane. The use of liposome as model bilayer systems allow the investigation of biological processes that occur at cellular level. Some examples are: viral attack, cellular signalling events or ligand-receptor phenomena.

The model can be improved if small unilamellar liposomes adhere and break at a surface forming a supported lipid bilayer. The immobilization of the lipid bilayer on a control surface permit a stable and deeper study. As a cell membrane model, the lipid bilayer retain two-dimensional fluidity and can be an excellent environment for presenting membrane proteins.

14. LIPOSOME AND SUPPORTED BILAYER CHARACTERIZATION

As a model of one of the most important structure in biology, liposomes are widely studied. There are a multitude of methods to characterize the size, the surface charge, the encapsulation efficiency, lamellarity etc. of liposomes. Some examples are fluorescence microscopy, atomic force microscopy, dynamic light-scattering, flow cytometry etc[30]. However, liposomes are biologic dynamic structures prepared to interact with the environment in which they are located. Some of interactions include the adhesion to some surfaces or even their rupture.

This interaction is especially useful to create supported lipid bilayers that, as mentioned before, are an excellent membrane model. However, the characterization of both structures and the transition between them becomes mandatory to have a reliable model. There are many techniques to perform this to perform this characterization[28,30,31] but between them the most relevant is the QCM.

This technique becomes perfect thanks to its capacity of cover the crystal with different coatings that foment the adsorption of liposomes and permit distinguish both structures thanks to their different shear acoustic properties .

Both lipid structures can be identified with frequency and dissipation changes as represented in figure 14. The defining characteristic that has allowed the differentiation between adsorbed liposomes and adsorbed bilayer is the capacity of dissipate energy. Liposomes are very flexible lipid structures that contain liquid and they will dissipate the shear waves. In the other hand, a lipid bilayer forms a thin film that will not dissipate the shear waves, and as a consequence, it will fulfill the Sauerbrey relation.

In conclusion, the key features that identify a liposome adsorption after the liposome injection are:

- Increase in Dissipation. The viscoelastic properties of the liposomes cause an energy loss.
- Decrease of frequency. The mass of the liposomes absorbed by the crystal will decrease the vibration frequency.

The key features that identify a lipidic bilayer adsorption after the liposome injection are:

- Increase and decrease in dissipation. The liposomes will be absorbed causing an increase in dissipation and then they will break forming a bilayer. As the bilayer has an elastic behavior, the dissipation will return to the same values of the beginning.
- Convex form in frequency. The frequency will decrease as the liposome adhere to the surface of the crystal. When a critical point of covering is archived, the liposomes will break forming a bilayer and the frequency will increase.
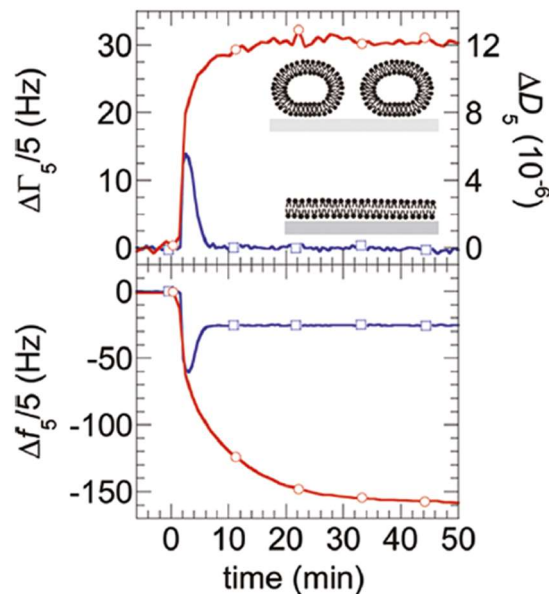
figure 13: figure extracted from reference [35] *Sensitivity of QCM to layer morphology is illustrated by the archetypical example of liposomes adsorbing on an inorganic surface. Liposomes are quasi-spherical lipid structures developed as cell membrane models. Red curves represent adsorption of intact liposomes to a surface. Blue curves correspond to a scenario where liposomes adsorb initially intact and later rupture into a planar lipid bilayer. In both cases, the surface is TiO2 and liposomes were made of dioleoyl phosphatidyl choline (red curves) and dioleoyl phosphatidyl choline containing 20% of dioleoyl phosphatidyl serine (blue curves). The differences between the two cases are quite striking: the liposome film causes a greater frequency shift than a bilayer. This happens because it is thicker. It also dissipates more energy, because it is laterally heterogeneous*

Keller was the first to measure the kinetics of lipid vesicle adsorption onto different prepared surfaces[32] on 1998. He found that lipid vesicle adsorption occurs in a qualitatively different manner on different types of surface   (SiO_2, tiholated gold and oxidized gold).

When the adsorption of liposomes occurs on a SiO_2 coated crystal and a critical surface of the crystal is covered, the liposomes will break forming a bilayer thanks to the high hydrophilic forces of the surface. On thiolated gold surfaces, the hydrophobic forces will be strong enough to form a phospholipid monolayer (with the tails in contact with the surface) when the liposomes reach the crystal. In the other hand, when the adsorption occurs on oxidized gold, the liposomes will adhere irreversibly and stably Thanks to the hydrophilic forces that are strong enough to adsorb the liposomes but too weak to break them and form a bilayer.
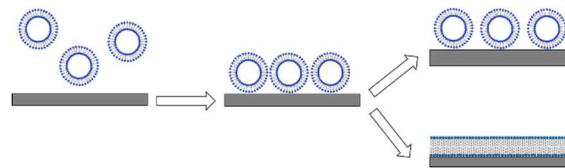
figure 14: *process of liposome adsorption. If the hydrophilic forces of the surface of the crystal are strong enough and a critical area of the surface is covered, the liposomes will break forming a bilayer.*

At this point the technique became really popular and several investigators continued working on the subject.

Some of the most important contributions were the first attempts to calculate the mass of the liposomes adsorbed [33] on 2002, the analysis of the influence of temperature, size and osmotic pressure in the process [34] on 2003 and the in-deep analysis of the adsorption nanomechanics[8] on 2009. A full review on the subject can be found here [35].

Right now, the appearing of high fundamental frequency crystals has opened a new way to analyze this well-known model and, at the same time, test the performance of this new sensors.

15. CHARACTERIZATION OF HFF CRYSTALS WITH BILAYER TRANSITION

As mentioned before, the advances in fabrication technology permitted the invention of new high fundamental frequency crystals thinner and more sensitive than regular ones. At this point several questions arrays about its performance. A well-known system such as the liposome transition to bilayer could be used to analyze what new information can be obtained of this process with the HFF crystals and, at the same time, compare the quality of these measurements with the regular crystals.

For this purpose, we will compare the liposome adsorption and its transition to bilayer on a crystal surface of 100 MHz coated with SiO_2 and a 5 MHz crystal in the same conditions.

The reasons to select this method are:

- Known liposome and bilayer characteristics: The size, mass, and thickness etc. of the liposomes and the bilayer is known.
- Good knowledge of adsorption characterization: there are a lot of works that use liposome adsorption and can be considerate as a standard test

- Permit perform the measurements in a liquid media
- Permit perform a noise and sensitivity analysis before the experiment.
- Transition between two QCM models: The first one corresponds to the liposomes, that form a heterogenic viscoelastic film. The second one corresponds to the lipidic bilayer, that form a homogenic elastic film, where the Sauerbrey relation is valid. The return to "zero" of the dissipation will determine the good performance of the experiment and the validity of the Sauerbrey relationship.

The experiment consists os coating a 5MHz and 100MHz crystals with SiO_2 to permit the breakdown of the liposomes when adsorbed forming a bilayer. The 5MHz crystal is used as a reference and as a "gold standard". Then, a continuous flow of liquid will pass to the surface of both sensors. At this point, the performance of the crystals in viscous media will be measured. After that, the small unilamellar liposomes will be injected. They will circulate in the flow and will be adsorbed on the surface of both crystals. When a critical area of the surface will be covered, the liposomes will break forming a bilayer. The frequency and dissipation changes during this process will be registered and compared.

Justification

The present Thesis is part of the master's final projects (TFM). The TFM is an academical exercise of which principal objective is confirming that the student has acquired the proposed skills on the master's context and is able to apply them to present justified solutions for the Thesis' suggested problems.

This thesis was conceived by the "centro de biomateriales e ingenería tisular" (CBIT) and the AW Sensors company. AW Sensors is a young Spanish company developing new sensing technology based on ultra-high frequency (150 MHz) shear-acoustic crystals.

AW Sensors applied for creative students interested in doing their Master projects in an industrial Research and Development (R&D) setting with the aim of answering the following question:

What is the performance of the high fundamental frequency crystals as crystals in QCM technique compared with normal ones when used to evaluate cell membrane models and what new nanomechanical information can they extract from them?

The strategies to solve this problem include biophysical and bioanalytical methods in relation to lipids and surfaces (liposome and bilayer preparation and characterization, surface preparation and characterization) to accomplish the objective of -as will be discussed below- investigating lipid systems with high-frequency acoustic sensors that are expected to provide new information about the nanomechanical and physico-chemical properties of these lipid systems, and to evaluate new sensor performance.

In the past, commercial and home-made sensors based on low-frequency (5 – 50 MHz) shear-acoustic crystals were used to study cell membrane models: assemblies of lipids in the form of solid-supported lipid bilayers or surface- adsorbed liposomes. Latest developments in this field include measurements of surface- adsorbed liposome deformation, surface-adsorbed bilayer and liposome mechanical properties, and detection of anaesthetics by monitoring lipid phase transitions.

This problem is particularly interesting to solve for its applications in both pure academic fields such basic lipid biophysics/cell membrane and biomaterials research and in more applied areas such as biosensor development because membrane models became the "de facto" industry standard for evaluating acoustic sensor performance.

For the student, the resolution of this problem allows to expose the knowledge acquired in: biophysics, biochemistry, nanotechnology, digital treatment of signals, electrical instrumentation, piezoelectric effect, lab and research skills, design of experiments, project management and deduction capacity.

Normative

The specific normative for the Spanish laboratories it's limited to the "Real Decreto 822/1993" and the "Real Decreto 1369/2000" which describe good laboratory practice. In addition to the specific laboratory normative, we should apply the appropriate non-lab normative that is relevant for our activities. To end, we used the normative of the "Universidad de València" labs for the preparation of liposomes and its characterization.

In particular, the normative applicable during the execution of the Thesis is the subsequent:

- Real Decreto 822/1993 "buenas prácticas de laboratorio y su aplicación en la realización de estudios no clínicos sobre sustancias y productos químicos"

- Real Decreto 1369/2000 "Modificación Real Decreto 822/1993"

- Ley 31/1995 "Prevención de riesgos laborales"

- Real Decreto 363/1995 "Reglamento sobre notificación de sustancias nuevas y clasificación, envasado y etiquetado de sustancias peligrosas.

- Real Decreto 1902/2008 "Modificación del Real Decreto 363/1995"

- Real Decreto 1215/1997 "Disposiciones mínimas de seguridad y salud para la utilización por los trabajadores de los equipos de trabajo"

- Real Decreto 486/1997 "Disposiciones mínimas de seguridad y salud en los lugares de trabajo"

- Real Decreto 374/2001 "protección de la salud y seguridad de los trabajadores contra los riesgos relacionados con los agentes químicos durante el trabajo"

- Real Decreto 833/1988 "Reglamento para la ejecución de la Ley 20/1986, Básica de Residuos Tóxicos y Peligrosos"

- Tareas de mantenimiento en laboratorios de investigación, docencia y experimentación de la universitat de València, València, 13 de Abril de 2016

Materials

1. **CHEMICAL REACTIVES**

In the table 2 the reagents used in the experiments are listed. The table indicates the name of the product used and the name of the company where it was purchased as well as its commercial reference.

Table 2: Chemical reagents

Chemical reactive employed	Commercial brand	Commercial reference
DOPC >99% (TLC)	Avanti Polar Lipids, Alabaster, Alabama.	850375P
HEPES ≥99.5% (titration)	Sigma-Aldrich, Madrid, Spain	H3375-100G
NaCl	Acros organics, Geel, Belgium.	42490010
$CaCl_2$	Sigma-Aldrich, Madrid, Spain.	C8106-500G
NaOH	Sigma-Aldrich, Madrid, Spain.	71690-500G
Chloroform	Sigma-Aldrich	–
Water for analysis	Panreac Química S.L.U., Barcelona, Spain.	131074.1214
Ethanol	Panreac Química S.L.U., Barcelona, Spain.	141086.1214
SDS	Panreac Química S.L.U., Barcelona, Spain.	–
Nitrogen	AIR LIQUIDE, Madrid, Spain.	–
Ultra-pure argon	–	–

2. EQUIPMENT

In the following table the devices and the most relevant materials used during the experiments are detailed. The table indicates the nature of the device or material, its commercial name and its manufacturer

Table 3: Equipment used

Equipment	Specifications	Manufacturer
Sonicator	Q500 Sonicator	Q Sonica, Newton, Massachusetts
Centrifuge	5418R refrigerated model	Eppendorf, Hamburg, Germany
pH meter	Hanna EDGE pH/OD/EC	Hanna, Eibar, Spain
Digital-analytical balance	Kern AES-C/AEJ-CM	Stuttgart, Germany
Flow system	AWS F20 Research platform	AWS, Valencia, Spain
Measurement platform for acoustic sensors	AWS A20 Research platform	AWS, Valencia, Spain
Network analyzer	Network analyzer Agilent E5100A	Keysight, Santa Rosa, California
Dynamic light scattering measure (DLS)	Zetasizer Nano ZS, Malvern	Malvern, Alcobendas, Spain
5 MHz QCM crystal	AWS 5 MHz quartz crystal coated with SiO2	AWS, Valencia, Spain
100 MHz QCM crystal	AWS 100 MHz quartz crystal coated with SiO2	AWS, Valencia, Spain
Flow conductivity measurement device	EDA in-flow conductivity measurement monitor	Biopac systems, Goleta, California
Ozone cleaner	UV Ozone Cleaner – ProCleaner	Bioforce nanosciences, Spillburg, Germany
Syringe filter 0.2 µm	Whatman FP 36/0.2 CA-S	GE Healthcare, Barcelona Spain

3. LAB EQUIPMENT

Table 4: Lab equipment used

Lab utensils
Beaker 250 ml, Micropipette, ISO flask 1L, spatula, nitrile gloves, stirring magnet, weighing paper, graduated cylinder, Hot plate, Dewar flask, 50 ml and 10 ml glass beakers, thermometer, tweezers, Eppendorf tubes, Hamilton microliter syringes, Pasteur pipettes, cell culture dish, test tubes, parafilm, syringe filters,

Methods

1. HEPES BUFFER PREPARATION

Overview

HEPES buffer solution is used in all of the experiments performed in this Thesis. Ca^{2+} was included in the buffer solution to favor the formation of a lipid bilayer[2]. The concentration of the chemical reagents can be found in table 5.

Table 5: HEPES Buffer composition

Composition of 7.36 pH HEPES 10 mM buffer	
HEPES	10 mM
NaCl	150 mM
$CaCl_2$	2 mM

Preparation

The chemical reagents were weighed with the analytical balance to achieve the desired concentrations and then dissolved in 50 ml of water in a beaker. After that, the pH of the solution was adjusted using NaOH to the desired value of 7.36. The resulting buffer solution was then diluted to the appropriate volume of 0.5 L. The buffer was stored at +4 C until used and filtered with a 200 nm syringe filter immediately prior to use.

2. DOPC LIPOSOME PREPARATION

Overview

Liposomes were prepared at the Membrane Biophysics Group, Instituto de Ciencia Molecular (ICMol), Univ. of València. according to a standard protocol previously employed in the laboratory of Dr. Ilya Reviakine [36].

We used 1,2-dioleoyl-sn-glycero-3-phosphocholine (DOPC) phospholipid to form liposomes.
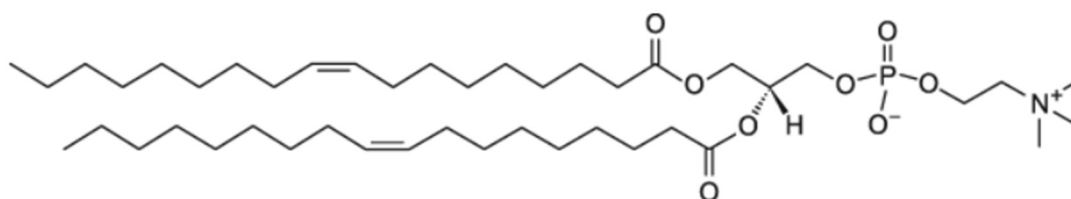
figure 15: *DOPC (1,2-dioleoyl-sn-glycero-3-phosphocholine) phospholipid molecule. Source: Avanti polar lipids INC.*

We prepared multilamellar vesicles (MLVs) by hydrating and swelling a dry phospholipid film prepared on the walls of a round-bottom test tube with the HEPES buffer solution. The swelling

process is speed up by agitation and the result is a milky suspension of MLVs several tens of microns of diameter. The conversion of MLVs into unilamellar vesicles can be achieved by a variety of methods, all of which have one thing in common: they entail the formation of an intermediate state, bilayered phospholipid fragments (BPFs). These fragments are formed through mechanical disruption of the MLVs bilayers. There are several ways to produce this disruption, in this Thesis we used sonication technique. The thermodynamic instability at the edge of BPFs causes them to bend and self-closing into SUVs (Figure 2).
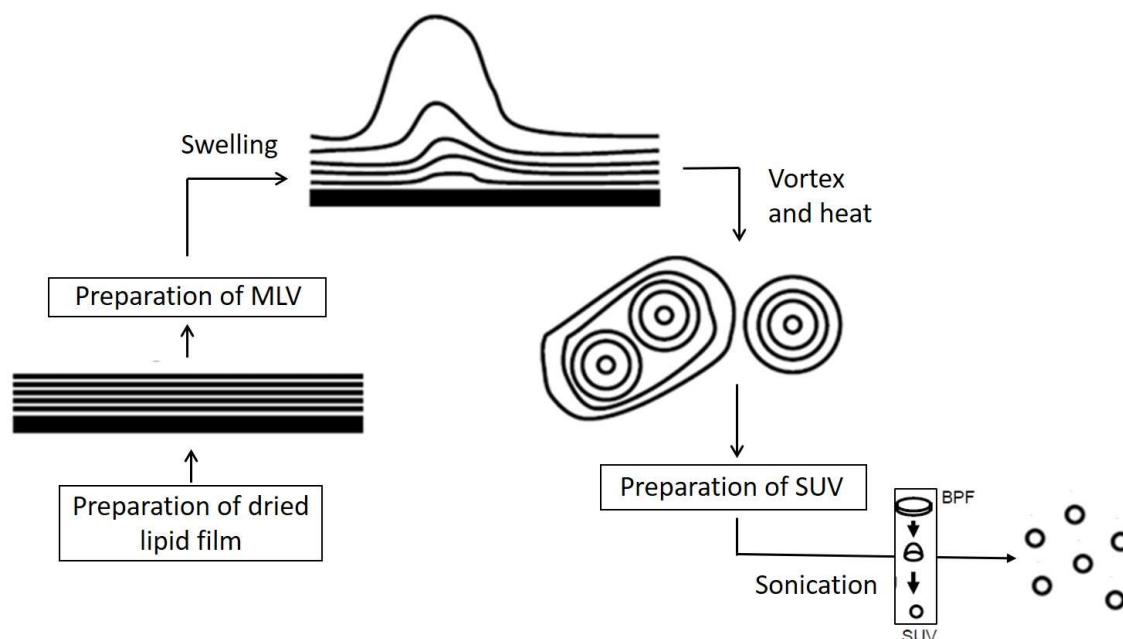
figure 16: *DOPC SUV preparation scheme. DOPC stock solution is dissolved in chloroform, then the dissolvent is evaporated. The dried film resulting is swelled with HEPES buffer forming multi lamellar vesicles (MLV). After that sonication is used to break the MLVs and form bilayered phospholipid fragments (BPFs) that will self-close and form small unilamellar vesicles (SUV).*

Preparation

Preparation of the dried lipid film:

We cleaned a Hamilton microliter syringe and a glass tube with chloroform. Then we deposited 2 ml of a solution of the 2mg/l DOPC chloroform solution into the cleaned glass tube using the Hamilton syringe. Next, we evaporated the chloroform using a stream of argon, creating a phospholipid film on the inner surface of the glass tube. When the chloroform was evaporated, the preparation of MLVs was started.

Preparation of MLVs:

Using 1ml of the previously prepared HEPES buffer, we hydrated the lipid film prepared above. Next, we created an argon blanket by gently blowing argon over the lipid suspension and then we sealed it using aluminum foil and parafilm. Then we mixed it using a vortex mixer. Since the main transition temperature of DOPC is − 17Cº according to the fabricator (Avanti), the preparation was performed at room temperature.

Preparation of SUVs using Sonication:

We disrupted MLVs with ultrasonic energy (sonication) to produce SUVs with diameters in the range of 25 – 100 nm.

First, we purged the cabin of the sonicator with nitrogen maintaining the nitrogen flow during the sonication. Next, we cleaned the sonicator's tip wiping it with ethanol and then run the sonicator in a beaker of Nano-pure water for 2-3 minutes. Then we assembled the test tube with MLVs in the sonicator.

The liposome suspension was immersed in an ice bath to minimize thermal damage to the lipids from the sonication. .

Sonication was performed under 30% of duty cycle, power 30, setting 3 for around 1 hour until the milky MLV suspension became transparent. Foam formation and splashing during sonication was avoided.

Titanium particles introduced in the lipid suspension by sonicator tip were removed by centrifugation at 22000 xg at 4 Cº under nitrogen.

3. DOPC LIPOSOME CHARACTERIZATION

Overview

We use Dynamic light scattering (DLS) to measure the size of the vesicles previously prepared and prove the uniformity and size of the DOPC liposomes produced.

Dynamic light scattering measurements assume that particles move due to Brownian motion in a medium of proportionately small molecules. When a particle is illuminated by a light source such as a laser, it will scatter light in all directions. The motion of the particles will cause the intensity of scattered light to fluctuate. Analysis of the time-dependent correlations between these fluctuations allows the diffusion coefficient of the particles in suspension to be calculated.

Zetasizer Nano ZS collects the intensity fluctuation data and then performs autocorrelation analysis to extract particle's diffusion coefficient D from the decay rate of the autocorrelation function. The diffusion coefficient is related to the particle size and the viscosity of the media by the Stokes-Einstein equation:

$$d(H) = \frac{kT}{3\pi\eta D}$$

In the equation: d(H) is the hydrodynamic diameter (evaluated); D refers to the translational diffusion coefficient (measured); k is Boltzmann's constant; T is the temperature and η is the viscosity of the dispersant (water, 0.89 cP).

Therefore, dynamic light scattering measurements report the hydrodynamic diameter, d(H), of the dispersed particles. For solid spherical particles, this corresponds to their actual diameter. Otherwise, it corresponds to the diameter of a sphere of equivalent volume.

Procedure

We used The Zetasizer Nano ZS to determinate two fundamental parameters: The Z-average, and the polydispersity index. The first one Is the accepted norm for presenting particle sizing results by DLS. The second one gives an indication of the width of overall distribution, assuming a single mean

The measures taken were made according to the user's manual. The fundamental steps taken were:

- Check if DLS cell is clean performing a measure of this cell filled with water
- Make 1ml of 0.2 mg/ml diluted vesicle sample with filtered and degassed buffer.
- Take out the cell from the cell area
- Dry the cell with Nitrogen
- Fill in the cell with 800 μl of diluted 0.2 mg/ml vesicles using the method mentioned above.
- Set parameters in Zeetasizer Nano ZS
- Put the cell into the cell holder
- Start the measurement
- Repeat the experiment with 3 different samples.

4. QCM EXPERIMENTS:

Overview

The experiment consists in create a constant flow of HEPES buffer through the QCM cells where the 100 MHz crystal and the 5 MHz crystal were mounted. Once stable conditions have been reached, DOPC liposomes will be introduced in the constant flow, coming in contact with the crystal surface and being adsorbed by it.
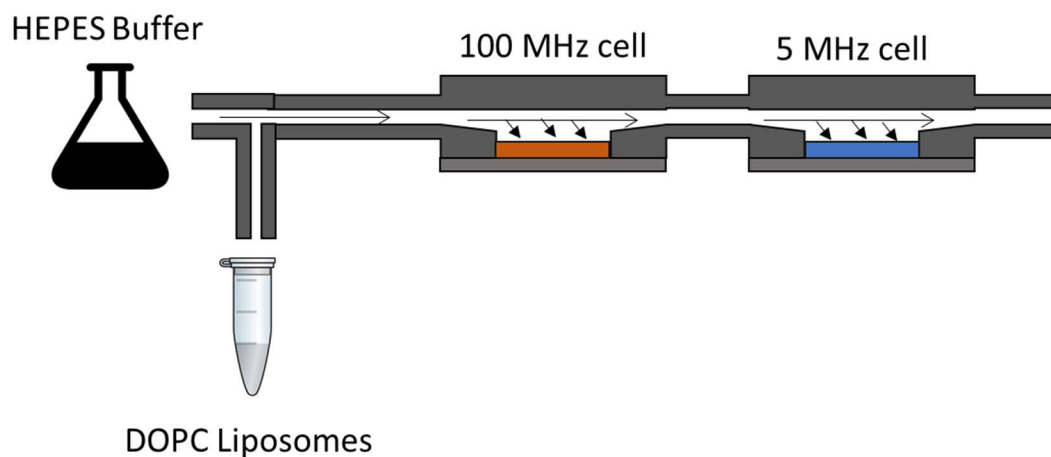
figure 17: *Schematic overview of the experiment: A constant flow of HEPES will circulate to the 100 MHz crystal (orange) and then to the 5 MHz crystal (blue). Then, the flow will leave the system ending in the waste. When the stable conditions are reached, the DOPC liposomes will be injected to the system.*

Quartz crystal crystals

5 MHz Crystal:

The 5MHz Crystal used is a design of AW sensors and the following properties are extracted of its technical file.

The sensors are coated with SiO_2 .

General

Sensor design	Plano-Plano
Cut	AT
Frequency vs Temperature stability	< ± 5 ppm (0 to +50ºC)

Electrical

Nominal Frequency	5.000 MHz
Center Frequency	4.960 MHz
Frequency tolerance	± 10 KHz
Q-value (in air)	> 100000

Mechanical & Electrodes

Nominal blank diameter	14.0 mm
Surface finish	Polished
Front electrode diameter	12.0 mm
Back electrode diameter	5.0 mm
Electrodes material	Cr/Au, Chromium / Gold
One sided contacting	Yes
Coating thickness	100 nm
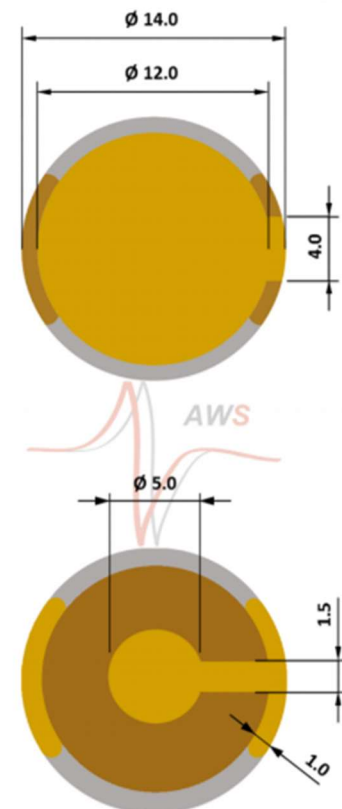
100 MHz Crystal:

The 100 MHz Crystal used its fabricated by Connor Winfield and sold by AW sensors.

There are AT-cut quartz crystals with a square profile with a total area of about 36 mm2 and a MESA region in the central part, where the thickness of the quartz is about 17 µm. In the central zone gold electrodes are deposited on each of the faces of the crystal. The extremely thin thickness of the sensor makes necessary the mounting of the sensor on a Poly-Phenilen Sulfide (PPS) support. These were coated with 15 nm of SiO2 by reactive magnetron sputtering at the Paul Scherrer Institute (PSI, Switzerland), according to the procedure described in[37]. Surface composition was characterized with X-ray photoelectron spectroscopy (XPS).
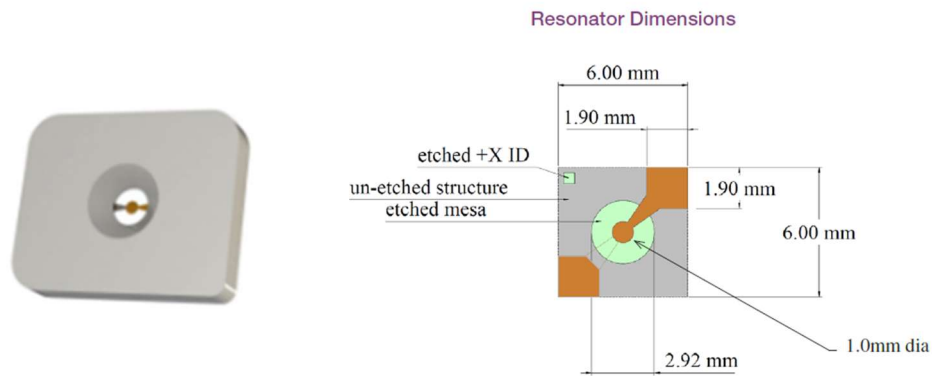
figure 18: *100 MHz crystal (left) and its dimensions (right)*

Flow cells

The previously described crystals were mounted into a flow cell. This cell on one hands connects the sensor to the measurement device (AWS A20 RP) and on the other hand allows the flowing of a controlled stream of liquid containing the liposomes above the sensor surface. The volume of the liquid in contact with the crystal will be $45 \, \mu l$ for the 5MHz cell and $5.5 \, \mu l$ for the 100 MHz cell.

The bottom part of the cell is fabricated in aluminum. The cell will be connected by the measurement device for its lower face. The crystal will be adjusted in the top face. Then, the top of the cell, fabricated of PMMA, will be used to close the crystal inside the cell. The upper part of the cell incorporates two fittings to connect the plastic pipes. The union between the two parts of the cell is achieved via a patented Quick-lock system.

The flow cells used in this Thesis are property of AW sensors.
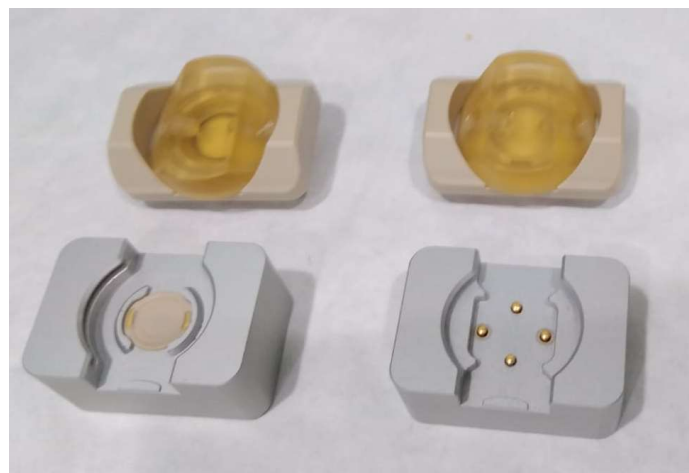
figure 19: *Flow cells: Upper part of the flow cell (top) with Q-lock system and 2 arrays for connect the plastic pipes. Aluminum base allows the connection between the AWS A-20 (lower face) and the crystal (top face). There will be a flow cell for 5 MHz crystal (left) and for 100 MHz crystal (right).*

AWS A20-F20 Research platform

AWS A20 RP (top device in the next figure) is a universal measurement platform for acoustic sensors specially designed for biological applications. It has 4 measurement channels, so it is possible measure at the same time with the 5 MHz cell and the 100 MHz cell. The platform integrates a thermostatic system that allows to minimize the noise of the measurement. It is based on the phase analysis readout method described in section XXX of the introduction. The device provides: the temperature inside the device, frequency changes, and dissipation changes.

The platform is mounted with an AWS F20 RP (bottom device Figure 20). AWS F20 RP is a flow system based on syringe bumping that provides a constant flow to the cells when connected with pipes. The platform consists in a syringe that provides a constant flow, a distribution valve to select the desired composition of the flow, an injection valve to load the sample and a sample pump to incorporate it to the flow.

Both platforms are prepared to work together and can be controlled with the AWSuite, a software created by AW sensors to control both platforms wireless and display the collected data.

figure 20: *AWS A20-F20 Research platform. Composed for an AWS A20 platform (top) where is possible see the 4 channels where the flow cells will be connected and an AWS F20 platform (down) where is possible to see the syringe, the distribution valve, the sample pump and the injection valve (bottom-top order).*

Network analyzer Agilent E5100A

The E5100A/B network analyzer is a 10 kHz to 300 MHz network analyzer used to replace the AWS A20 platform and validate the results obtained with it.

figure 21: *network analyzer Agilent E5100A*

AWS Suite

AWS suite software is an intuitive, fast and simple interface that allow the management of multiple AWS A20 systems and AWS F20 fluidics module from a single interface. Furthermore, the software allows remote access to devices by IP address within the network. AWS Suite organizes all the data in a file system based in the creation and management of projects. The program permits the exportation of the data to other formats, such as ".xls".
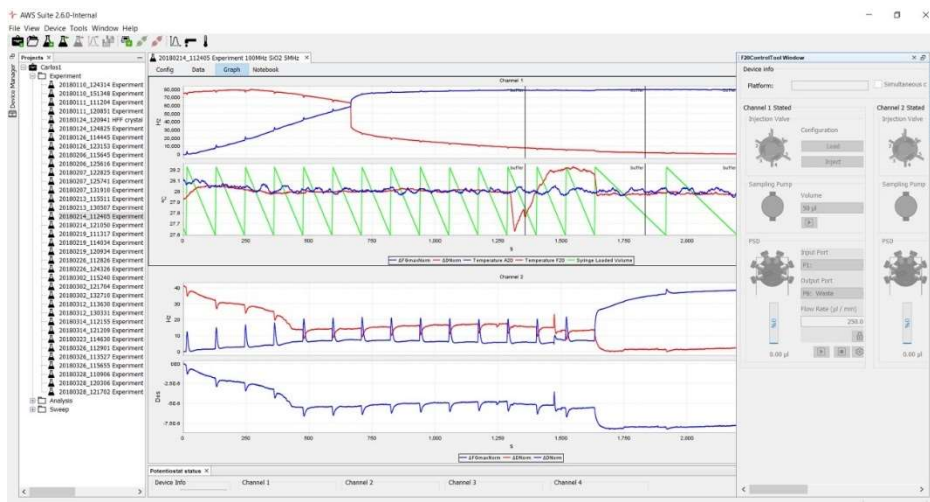
figure 22: *AWS Suite interface. From the left to the right: project file with all individual experiments. Plotted results of both cells (100 MHz and 5 MHz) frequency and dissipation (red and blue) and syringe volume (green) with AWS A20 temperature (blue) and AWS F20 (red) temperature. Flow control of the AWS F20 (right).*

Procedure

A schematic view of the fluidic plumbing of the F20 is shown in ?FIGURE?. The flow of liquid (water or buffer) is driven by a multi-port syringe pump. This liquid expelled from the syringe follows the path from the distribution valve to the sample injection valve and ultimately to the measurement cell, either directly (if the injection valve is in load position) or through the sample injection loop (if the valve is in the "inject" position).

For introducing liposomes into the experiment, they are loaded into the sample injection loop
through the aspiration tubing connected to the port number 4 of the injection valve..
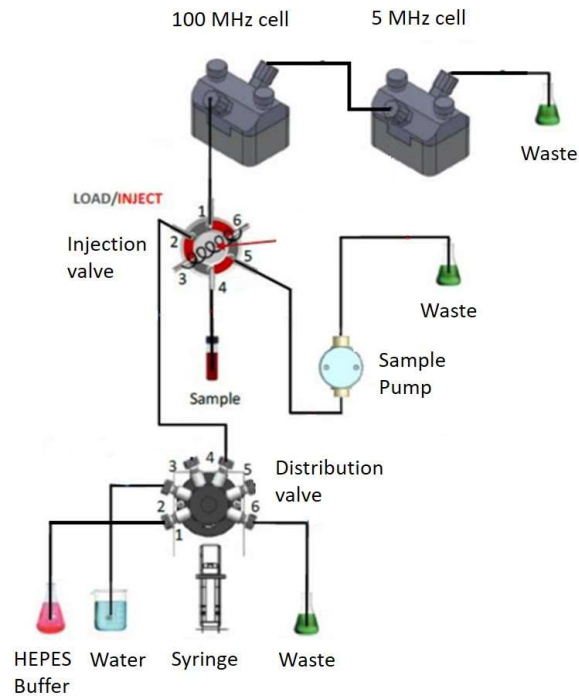
figure 23: *Experimentation scheme. The syringe will create a constant flow absorbing HEPES or water. The origin and destiny of this flow will determine by the distribution valve. The sample pump will load the sample into the spiral tube that connect the ports 3 and 6 of the injection valve. When the injection valve change to the "inject position", the spiral tube will become part of the circuit. Then the flow will continue to the crystals cells and finishing at the waste.*

The experimental process can be divided in several subprocesses, as described in figure 9. The procedure will be determined by the need for stability and homogeneity on the liquid flow and the surface of the crystals. When measuring structures of 30-60 nm of diameter, all contaminant particle of similar size that can be absorbed by the crystal surface or even micro-sized bubbles can have a big impact in the final measure. For this reason, most steps of the procedure will be directed to the cleaning of the crystals and the machine.
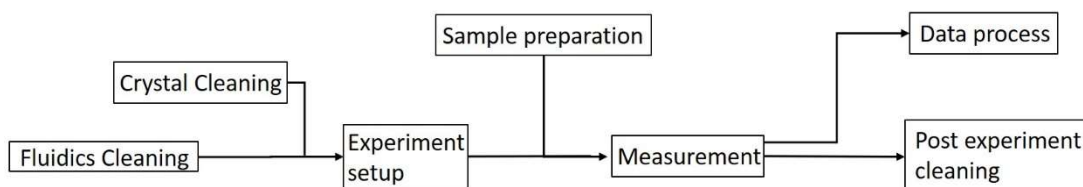
figure 24: *schematic of the experimental procedure: The experiment begins with the cleaning all the pumps, valves and pipes. Then the flow cells and the crystals will be clean. After that, the crystals will be mounted into the flow cell and connected to the fluidics and the AWS A20 measuring platform. The flow will flood the cells and the experiment setup will begin. After the baseline is reached the liposome sample will be prepared. In these conditions the measurement will begin, and the liposomes will inter in the constant flow. After that,*

*all the fluidics and crystal should be cleaned for the next experiment. To finish, the collected data will be
exported for its later process*

Fluidics cleaning

Overview

Cleaning of the fluidics of the system is crucially important due the nature of lipid-surface
interactions, as the success of the bilayer formation depends on the surface properties. Bilayes
form on clean SiO2 but not on contaminated surface.

Procedure

Starting for the "dirtiest point" of the measurement system, the plastic tubing of the upper part,
as is shown in figure 23, connecting the injection valve to the fluid cells, every tube will be
disconnected and rinsed with water, ethanol, and again water, using a syringe. This operation
was performed before every experiment.

When the manual cleaning step is finished, the automatic cleaning will start. Using the control
software of the AWS 20F RP, water is run through the various fluidic paths of the equipment
(port 1 to port 6, port 2 to port 6, port 2 to port 3, etc.) for various time periods. After the
cleaning, the sample tubing is dried with nitrogen.

The injection valve and the sample injection loop is cleaned with water from an Eppendorf using
the sampling pump. The injection valve is cleaned by periodically changing its position from load
to inject..

For testing the correct cleaning of the fluidics, a conductivity measurement is performed with
EDA in-flow conductivity measurement monitor connected to the pipes that exit from the port
1 of the injection valve. If the conductance is low (<0.05), the machine will be considered clean.

crystal cleaning

Overview

Cleaning the surface of the crystals and the flow cells is a vital process after the measurement
begin.

Procedure

The 5 MHz and 100 MHz quartz crystals are submerged for half an hour in a solution of SDS in a
cell culture dish. After that, the crystals are rinsed with water, dried with nitrogen, and then
introduced for half an hour into a UV-ozone cleaner.

At the same time, the upper part of the flow cells is cleaned with water-ethanol-water and then
dried.

When the ozone cleaner finishes, the crystals are mounted in the flow cells. The experiment is
started as soon as possible thereafter (< 1 minute) to avoid surface contamination of the crystals.

Experiment setup

Overview

After the cleaning, the flow cells with the crystals inside are mounted into the sensing platform and connected to the flow. The measurement starts and continues until the baseline is reached.

Procedure

The flow of water is stopped, and the flow cells are mounted in the AWS A20 platform (channel 1 for the 100 MHz crystal and channel 2 for the 5 MHz crystal). After that the flow is reestablished but using buffer (channel 2 of the distribution valve). Once the cells are filled with buffer and no bubbles are observed, the AWS suite is used to start the measurement.

Following the same procedure that in fluidics cleaning an Eppendorf with HEPES buffer will be prepared and absorbed by the sample pump to flood all the sample injection loop. When a baseline in the measurement is archived, we will change the mode of the injection valve to "inject" to incorporate the content of the spiral tube to the flow. At this point, no changes in the resonance frequency or the dissipation should be observed. This is performed to check the correct performance of the fluidics of the platform. After performing the injection of buffer 2 times, the liposomes can be injected.

Sample preparation

Overview

Dissolution of DOPC liposomes in HEPES in an Eppendorf.

Procedure

From the start concentration of 5 mg/ml of previously prepared DOPC liposomes, a concentration of 0.1 mg/ml in a volume of 1 ml is prepared in an Eppendorf.

This Eppendorf is the final sample and will be used during the measurement.

Experimental measurement

Overview

The liposomes are aspirated by sample pump and will into the sample injection loop and introduced into the fluidics by the injection valve. They then flow over the surface of the crystal and adsorb, resulting in changes in the frequency and dissipation. Under the right conditions, they will break down forming a bilayer.

Procedure

The Eppendorf with the sample is included in the fluidics and absorbed into the spiral tube by the sample pump. Changing the position of the injection valve the liposomes will enter in the

constant flow reaching the crystals, being adsorbed and then breaking forming a bilayer. This change will be registered by the AWS A20 measurement platform.

Post cleaning

Overview

After performing the experimental measurement, the surface of the crystals and the fluidics should be cleaned to eliminate the remaining lipids.

Procedure

The flow of buffer is stopped, and the flow cells are decoupled. The crystals are introduced again in SDS and the top of the flow cells cleaned with water-ethanol-water. The water flow is restored for half an hour to clean the remain liposomes in the tubbing.

Data processing

Data was exported from AWS suite and analyzed with EXCEL and MATLAB.

Results

1. GENERAL OVERVIEW

As previously discussed, the objective of this thesis is to compare the performance of 100 MHz QCM sensors (HFF) with that of the classical 5 MHz sensors and to analyse the properties of lipid layers with HFF sensors by evaluating the absorption and transformation on their surfaces of cell membrane models based on small (20-100 nm) DOPC unilamellar liposomes.

For this purpose, we prepared DOPC liposomes and SiO2-coated 100 MHz QCM sensors (not commercially available); commercially available SiO2-coated 5 MHz sensors were used. We then studied the interactions between DOPC liposomes and the two sets of SiO2-coated sensors in parallel, thus allowing a direct comparison between the two sets of sensors. Two variables were measured in the experiments: frequency and dissipation, as a function of time. The measurements were performed using the multichannel AWSensors A20 QCMD research platform connected to the F20 fluidic system visible in figure 20.

An example of an experiment is shown in the Figure 25. The experiment could be divided into three phases: The stabilization phase, the stable baseline phase and the experiment phase. During the stabilization phase, the two signals vary as a function of time asymptotically reaching stable values.
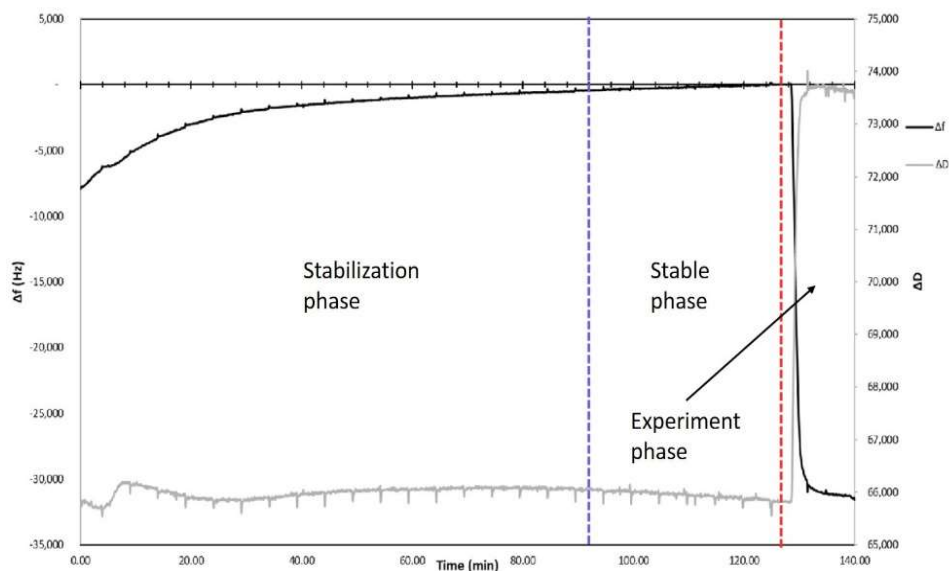
figure 25: *Overall HFF-QCM experiment performed with 100MHz crystal to measure the adsorption of DOPC SUV on its surface. The experiment is divided in three phases. The first correspond to the stabilization phase, where the crystal liberate stress until reach a stable baseline. After reaching the baseline, the experiment will enter the stable phase, where the sensitivity and LOD measurements will be performed. The liposomes will be injected, and the experiment will enter into the experiment phase, where the consequences of the liposome adsorption will be measured. The experiment will end when the new baseline will be established.*

Once the stable values of the two signals are reached, they are recorded for a minimum of 15 minutes (stable phase). This is called "baseline".

Experiment proper begins with the injection of the liposomes. The decision of injecting the liposomes is arbitrary and is done when the investigator believes that a stable baseline is reached and can be maintained for at least 15 minutes, and is unaffected by injections of blank buffer (without the liposomes). In Figure 25 after 30 mins of baseline, the liposomes are injected, and the experiment begins. The experiment is terminated when the signals after liposome injections stabilize at asymptotic values unaffected bu further liposome injections..

2. EXPERIMENT VALIDITY AND COMPARATION

We used the liposome breakdown into a bilayer because the transition between a dissipative structure, (liposomes), to a non-dissipative structure (bilayer), permits the validity of the Sauerbrey relationship to be affirmed at high frequency.. If the Sauerbrey relation is valid, the final frequency values can be used to obtain the mass of the bilayer adsorbed, making possible to directly compare the mass perceived by the 100 MHz crystals and the 5 MHz crystals.

5 MHz crystals are used at the same time as the 100 MHz crystals to prove the validity of the experiments comparing the results obtained with these crystals with the literature on the subject. If the frequency and dissipation changes in the 5 MHz crystal are similar to the literature values and the 100 MHz crystal is in the same conditions that the 5 MHz crystal (connected to the flow system in series with the 5 MHz crystal) we can infer that the same phenomena are happening in both crystals.
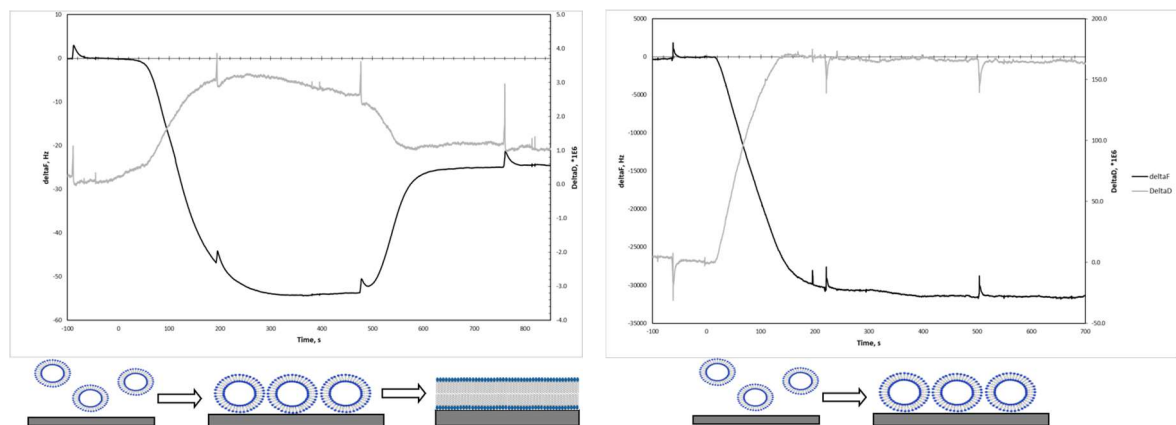
figure 26: 5 MHz QCM measurements for 3 injections of $250 \mu l$ DOPC SUVs $0.1 \frac{mg}{ml}$. Black lines represent the frequency change Δf, and the grey lines represents the dissipation change. Left image shows a bilayer formation after a critical surface of the crystal has been covered by the liposomes. On the right, the liposomes don't break and remain attached to the crystal surface

During the experiments two types of reactions were obtained using the 5 MHz crystals. One example of each is shown in figure 26.

In the first one, after a liposome injection, frequency decreased and dissipation increased. Subsequent liposome injection triggered an increase in frequency and a decrease in the dissipation. The final values for the frequency and dissipation shifts were ~ -25 Hz and ~ 0, respectively. This is the case shown in Figure 26a, while the exact values and statistical analysis of multiple experiments is presented below.

In the second case, liposomes injection triggered a decrease in frequency reaching -90 Hz and increase in dissipation. These conditions didn't vary when more liposomes were injected. This is the case shown in Figure 26b.

Based on the previous work of Keller and Kasemo [32] and Richter et al.[28] these two caes correspond to bilayer formation and liposome adsorption, respectively. In the first case, liposomes adhere to the surface and remain attached until enough surface of the sensor is covered with the liposomes, at which point they break forming a supported lipid bilayer (SLB).

In the second case, after liposome adsorption, there is no breaking. Instead, liposomes remain attached to the surface forming a layer on the surface (surface vesicular layer, or SVL). This happens when the surface of SiO2 is contaminated and the experiment therefore fails.

The spikes in the figures correspond to the pressure changes associated with filling of the syringe.

In the following sections, the results of the liposome adsorption and the crystal performance in viscous media will presented separately. The crystal performance was analyzed during the baseline section of the experiment, while liposome behaviour during the subsequent time after the liposome injection. We start with the analysis of crystal performance.

3. HFF-QCM SENSOR RESPONSE IN VISCOUS MEDIA

In this section the 100 MHz crystal performance in constant flow conditions of HEPES buffer during the stable phase will be compared with the 5 MHz crystal in the same conditions. The performance of the sensors is evaluated by analyzing the noise of the baseline region for the 100 MHz and 5 MHz sensors to establish the limit of detection LOD and comparing the results with the theoretical predictions based on the Quality Factor of the sensors. LOD is established by calculating the Allan deviation ($\sigma_y(\tau)$) and the root mean square (RMS).

The objective of these measurements is comparing the performance of the used crystals in liquid media with the values in the bibliography.

4. CHARACTERIZATION OF THE CRYSTALS

We calculated the quality factor of the 5 MHz and 100 MHz crystals (Table 7).

Table 6: Q-factor and bandwidth for the 5 MHz and 100 MHz crystals

Frequency (f_0)	Q-factor (10^3)	N
5 MHz	6.75 ± 3.03	8
100 MHz	0.49 ± 0.21	11

5. NOISE ANALYSIS

A noise analysis was performed to know the minimum mass that the system can detect in this media.

The instantaneous frequency given by the crystals was measured in function of time and can be represented as:

$$f(t) = f_0 + \Delta f(t)$$

Where $\Delta f(t)$ represents the frequency fluctuation, i.e. noise, and f_0 represents the theoretical frequency of the crystal in this particular media.

The instantaneous relative frequency variation, $y(t)$ can be defined as:

$$y(t) = \frac{\Delta f(t)}{f_0}$$

The relative frequency variation is used to compare the performances of oscillators with different fundamental frequencies.

The frequency stability can be characterized in the frequency domain or the time domain. The time domain characterization is usually used because it can determine the stability of oscillator in a given time interval (τ) which is the usually the quantity of interest during QCM measurements.

There are several ways to analyze frequency stability (noise). The most popular measurements are the Allan deviation and the root mean square (RMS).

In the following sections, the Allan deviation and the root mean square were calculated.

6. ALLAN DEVIATION

The Allan deviation is used as a standard of stability measurement in the time domain in several papers that study QCM noise[38] . Can be defined as:

$$\sigma_y^2(\tau) = \frac{1}{2} \langle (\bar{y}_{k+1} - \bar{y}_k)^2 \rangle$$

This variance is calculated with respect to the averaging time , as the noise is a function of the averaging time (measurement time).

The Allan deviation is used as a standard of stability measurement in the time domain. The oscillator detection limit, i.e., the smallest frequency deviation that can be detected in presence of noise is equal to

$$\Delta f(\tau) = \sigma_y(\tau) * f_0$$

The mass resolution can be obtained by the relationship between the detection limit and sensitivity by:

$$Resolution = \frac{\Delta f(\tau)}{S_c * f_0{}^2}$$

Where S_c is the Sauerbrey constant defined in the introduction. And τ is the averaging time used
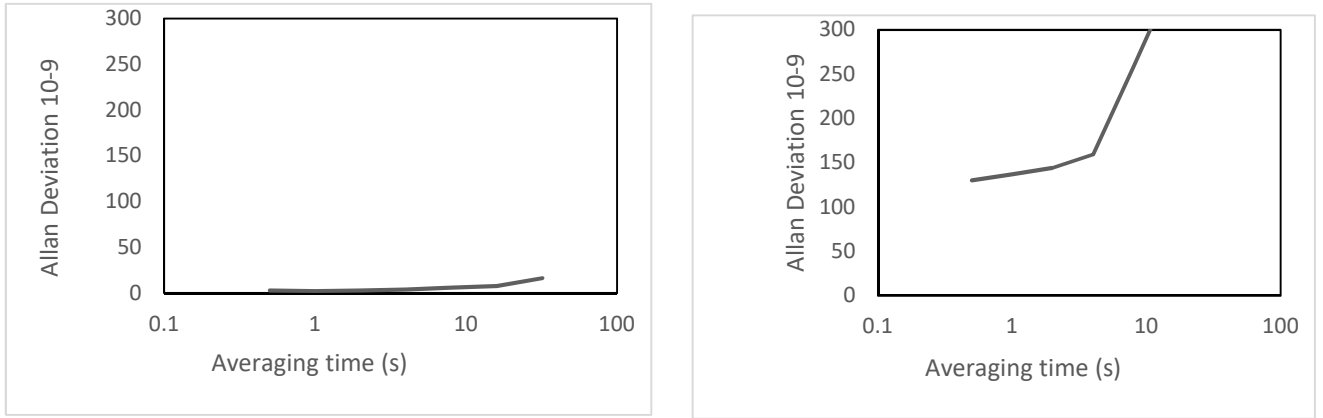
figure 15: Allan deviation calculated for a 5 MHz quartz crystal (left) and a 100 MHz quartz crystal (right)

In table 8 is presented the minimum Allan deviation $\sigma_y(\tau)_{min}$, the smallest frequency change detected $\Delta f(\tau)_{min}$ and its corresponding resolution in each crystal.

Table 7: Allan deviation characteristics

Crystal	$\sigma_y(\tau)_{min}$	$\Delta f(\tau)_{min}$	$Resolution\ (ng/cm^2)$
5 MHz	$2.4 *10^{-9}$	0.012 Hz	0.21
100 MHz	$130.1*10^{-9}$	14.0 Hz	0.56

We found that that the resolution is more than two times better for the 5 MHz crystal.

7. ROOT MEAN SQUARE (RMS)

Allan deviation is a measure that permits characterize crystals in a certain media and is the main tool to calculate the resolution of a crystal from the point of view of the electronics design. However, during the experiments, is necessary perform fast resolution analysis that didn't require too much data processing and interpretation. For this purpose, the root mean square (RMS).

The RMS is a statistical method used to estimate how far on average the error is from 0.

$$RMS = \sqrt{\frac{1}{N}\sum_{i=1}^{N} x_i^2}$$

This measurement result much more flexible than the Allan deviation and permit avoid the non-stationary noise. In this case, based in previous experiences, the sample contain 500 points and will be sited 5 minutes before the experiment start, as is shown in the figure 16
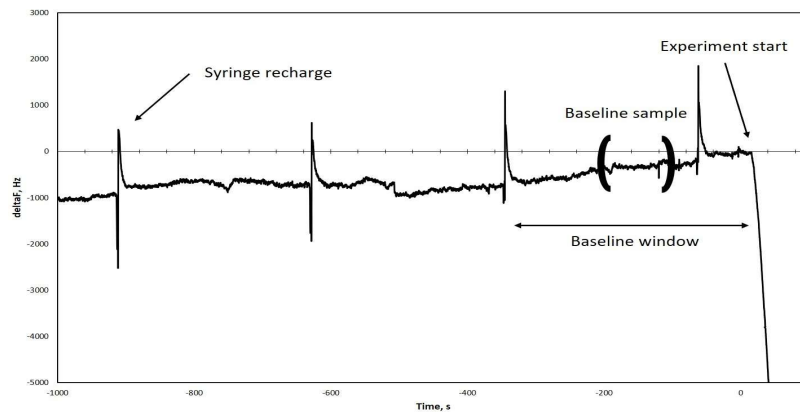
figure 16: Process of determining the sensitivity. A baseline sample of 500 points was selected in a window of 300 seconds after the experiment start. That window is equal for all experiments and it's done to avoid the spikes caused by the syringe recharge

In the context previously discussed, when selecting as sample the baseline previous to the start of the experiment, the limit of detection (LOD) will be equal to the root mean square:

$$LOD_\tau = RMS_\tau$$

The mass resolution can be obtained by the relationship between the detection limit calculated with the RMS and sensitivity "*S*" by:

$$Resolution = \frac{LOD}{S}$$

The next table show the standard error of the mean and its corresponding resolution for the 100 MHz quartz crystals. 2 different crystals where used. The experiments are ordered chronologically.

Table 8: 100 MHz Crystal characteristics calculated with RMS

Reference	$RMS_{500}(Hz)$	$Resolution_{500}(ng/cm^2)$	Crystal
ex219a	43.7	1.93	1
ex219.2a	25.1	1.11	1
ex220a	21.3	0.95	1
ex221a	53.0	2.36	1
ex222a	45.6	2.03	1
ex206a	248	11.2	2
ex207a	409	18.3	2
ex213a	214	10.9	2
ex226a	40.3	1.79	2
ex302a	79.1	3.53	2
mean	117 ± 129	5.41 ±5.94	

In table 10 the standard error of the mean and its corresponding resolution of the 5 MHz crystals are shown.

Table 9: 5 MHz Crystal characteristics calculated with RMS

Reference	$RMS_{500}(Hz)$	$Resolution_{500}(ng/cm2)$
ex206b	0.055	0.98
ex207b	0.101	1.82
ex214b	0.126	2.27
ex219b	0.560	10.1
ex222b	0.106	1.91
ex226b	0.869	15.6
ex302b	0.075	1.34
ex312b	0.024	4.31
Mean, 5 MHz	0.24 ± 0.3	4.79 ± 5.28

We find that the resolution is almost equal for both type of crystals when calculating the resolution with the RMS method.

Finally, for check the 100 MHz results obtained, we used the Network analyzer Agilent E5100A as an analysis platform and realized the experiment ex403a. Then we calculated again the Allan deviation and the root mean square. The machine had an acquisition frequency of 0.1 Hz.

Table 10: experimental resolution check

ex403a	$\Delta f(t)\ (Hz)$	$Resolution\ (ng/cm^2)$
RMS_{50}	37.7	1.46
Allan $\Delta f(\tau)_{min}$	15.2	0.6
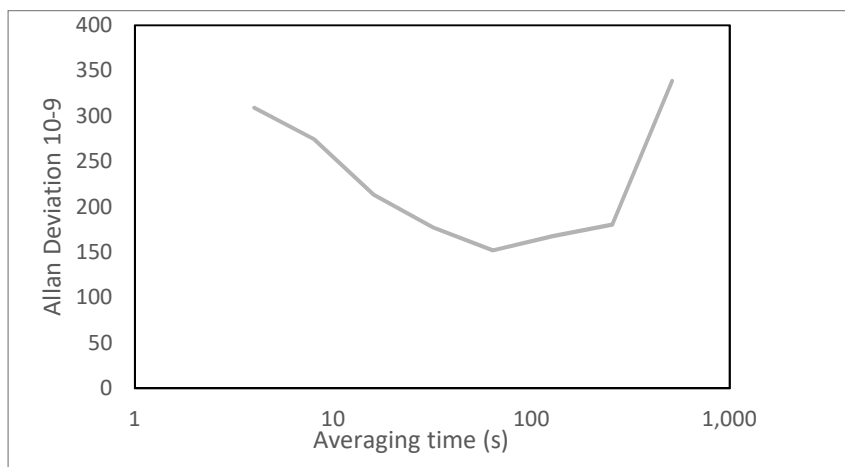
figure 18: Allan deviation calculated for the experiment ex403a using the the Network analyzer Agilent
E5100A

8. EXPERIMENT QUALITY AND OVERVIEW

QCM experiments are complex and time consuming. it's quite usual for experiments to fail
or have drifts, bubbles etc. Sometimes this defects not invalidate all the experiment but
make it more difficult to interpret. For this purpose, quality label is added to clarify the
level of formal validity that have the experiments. The quality of the experiments has
been classified between bad, ok and good.

1. Good Quality: A good baseline is archived. The experiment is coherent with
   literature values and the noise level doesn't interfere in the experiment
   interpretation

2. Ok Quality: The information collected by the experiment is valid, but some
   inconveniences occurred during the experiment such a drifts or bubbles
   makes the data less accurate.

3. Bad Quality: Although the lipidic structures could be characterized using the
   mentioned criteria, the inconveniences occurred during the experiment
   were critical. The experiment has a qualitative value, but the collected data
   is very inaccurate and only have qualitative valued.

Bubbles are the main reason of failure for QCM experiments. Occasionally, bubbles will
appear in the flow. The explanation of his appearing is complex, sometimes the syringe
will absorb air and incorporate it to the air. Other cause could be the formation of this
bubbles in the pipes of the machine due the air trapped on them. The formation bubbles
are a matter of time. The faster the experiment, the less chance of its generation. Other
important point to avoid bubble appearing is the correct cleaning of all the pipes,
especially the ones where the liposomes will circulate. Liposomes adhered to the walls of
the pipe can favour the bubble appearing.

The impact of bubbles in the experiment will depend in its size and the place where will be absorbed. When adsorption occurs away from the centre of the crystal and its size is
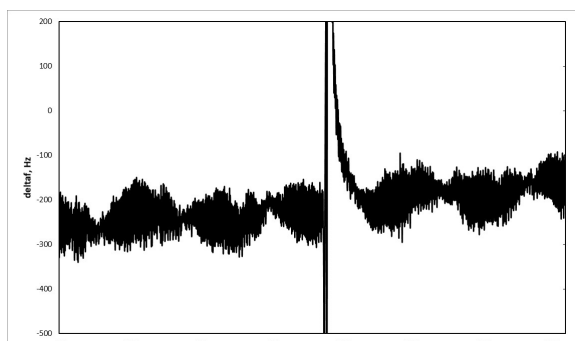
figure 17: Noise induced by a bubble in a 100 Mhz
crystal

reduced, only an increase in noise will be detected. In other hand, when the crystal has reduced dimensions, like the 100MHz crystal, all bubble appearing will be catastrophic

A summary of all experiments is presented in table 12:

Table 11: Experiment summary

Reference	Fundamental frequency (MHz)	Nº of crystal	Analysis platform
ex219a	100	1	AWS A20
ex219.2a	100	1	AWS A20
ex220a	100	1	AWS A20
ex221a	100	1	AWS A20
ex222a	100	1	AWS A20
ex206a	100	2	AWS A20
ex207a	100	2	AWS A20
ex213a	100	2	AWS A20
ex226a	100	2	AWS A20
ex302a	100	2	AWS A20
ex403a	100	3	Agilent E5100A
ex124b	5	-	AWS A20
ex206b	5	-	AWS A20
ex207b	5	-	AWS A20
ex214b	5	-	AWS A20
ex219b	5	-	AWS A20
ex222b	5	-	AWS A20
ex226b	5	-	AWS A20
ex302b	5	-	AWS A20
ex312b	5	-	AWS A20

Every experiment was coded with a reference number, for example "ex213". The number was assigned chronologically. 11 experiments using 100 MHz crystal were performed. 3 different crystals of 100 MHz were used in these experiments. To confirm the data obtained, another analysis platform was used in the last experiment (ex403a). The frequency of data acquisition is 10 Hz.

9. LIPOSOME PREPARATION AND CHARACTERIZATION

Small unilamellar vesicles (SUV) of DOPC were prepared and characterized.

The preparation of this vesicles was according to the liposomes preparation script previously mentioned. In order to check the validity of the prepared samples a Dynamic light scattering (DLS) test was performed. The outcomes of this test were:

- Zeta average: Is the result of analyzing DLS data using the technique of cumulants. Is the accepted norm for presenting particle sizing results by DLS.

- polydispersity index(PDI): PDI gives an indication of the width of overall distribution, assuming a single mean. Considering a Gaussian distribution, PDI = (w)2 where w is the width of the sample and w is the average of the sample.

Table 12: DOPC liposome characterization

Sample Name	T (CÂº)	Z-Average(d.nm)	PdI
20171211 BSUVs 1	25	61.22	0.261
20171211 BSUVs 2	25	61.15	0.262
20171211 BSUVs 3	25	60.45	0.26
20171211 BSUVs 4	25	61.47	0.266

The resulting liposomes have a size between 20 and 100 nm, in other words, they are small unilamellar vesicles (SUV).

DOPC SUVs were used at a concentration of 0.1mg/ml.

10. LIPOSOME BREAKDOWN WITH HFF-QCM

After reach a stable baseline, a volume of $250 \mu l$ of DOPC SUVs on HEPEs was injected. This operation will be repeated two more times waiting 5 minutes between injections. The successive injections will certificate that all the crystal is covered an inject more liposomes will not produce any change. Due the reduced dimensions of the 100 MHz crystal, only one injection is enough to cover all the surface. In other hand, 5 MHz crystal needs to 2 injections to trigger the break of the liposomes due its bigger surface.

In this section the data obtained after performing the experiments are presented. The frequency change (Δf) and the dissipation change (ΔD) will be calculated obtaining a baseline in the previous instants before the liposome injection and the baseline archived after the last injection of liposomes is done. The maximum dissipation (Max D) will be archived in the instants after the concentration of liposomes are critical on the crystal surface and before they start to

break forming a bilayer and decreasing the dissipation. Mass will be calculated using the Sauerbrey equation and the corresponding sensitivity (inverse of the Sauerbrey constant "C") for each crystal.

$$\Delta f = -\frac{1}{C}m_f = -\frac{1}{C}\rho_f d_f$$

Being ρ_f and d_f the density of the film and its thickness. For a bilayer film, the density will be due its high hydronation.

The characterization of the structures absorbed by the 100 MHz crystals will be discussed in the next chapter.

Table 13: Experimental results

Index	f_0	Δf (Hz)	Mass (ng/cm2)	ΔD (*1E-6)	Max D (*1E-6)	Quality	Structure absorbed
ex219a	100	-10524	441.41	4.04	24.4	Good	Lipidic bilayer
ex219.2a	100	-10666	447.37	4.28	20.9	Good	Lipidic bilayer
ex220a	100	-11142	470.43	3.19	15.9	Bad	Lipidic bilayer
ex221a	100	-11116	469.17	8.13	35.4	ok	Lipidic bilayer
ex222a	100	-23899	1008.6	117	117	Good	Liposomes
ex206b	100	-31325	1327.6	163	173	Good	Liposomes
ex207b	100	-11098	470.19	9.82	30.2	ok	Lipidic bilayer
ex213b	100	-16338	692.36	25.6	41.2	Bad	Liposomes
ex226b	100	-9693	409.26	3.78	30.7	Good	Lipidic bilayer
ex302b	100	-12706	537.68	36.1	104	Bad	Lipidic bilayer
ex403c	100	-31181	1327.3	153.3	157.4	Good	Liposomes
ex124	5	-23.6	401.64	0.40	1.84	Bad	Lipidic bilayer
ex222	5	-25.6	437.30	-0.26	3.21	Good	Lipidic bilayer
ex206	5	-25.5	434.45	1.06	2.25	ok	Lipidic bilayer
ex214	5	-24.5	417.61	1.07	3.19	ok	Lipidic bilayer
ex219	5	-23.9	408.01	0.83	2.15	Good	Lipidic bilayer
ex226	5	-17.5	297.30	-2.92	1.97	Bad	Lipidic bilayer

Discussion

In this work, the performance if the 5 MHz and the 100 MHz crystals was compared with each other with respect to mass resolution and the ability to detect the transition between liposomes and lipid bilayers. These results are now discussed in some detail.

1. SENSITIVITY AND NOISE COMPARATION

We found that the limit of detection and sensitivity is really similar for both crystals. We expected a sensitivity 400 times higher for the 100 MHz crystal according to the Sauerbrey relation. However, as said in point 5 of the introduction, "noise in QCM experiments", there is two types of noise: resonator noise and phase noise.

Table 14: Comparation between the Q-factor and the limit of detection calculated by Allan deviation and root mean square of both crystals

Crystal	Q-Factor (10^3)	$Allan\ LOD$ (ng/cm^2)	RMS LOD (ng/cm^2)
5 MHz	6.75	0.21	4.79
100 MHz	0.49	0.56	5.41

As is shown in table 14, the limit of detection obtained with Allan deviation it is smaller than the LOD obtained with the RMS method. That means that some resonator noise can be avoided using better acquisition techniques. However, the major part of the 100 MHz noise is not situated in the resonator. The Allan deviation LOD is 2 times bigger for the 100 MHz crystal than the 5 MHz crystal when it should be 400 times smaller. That means that the major part of the 100 MHz sensitivity loss is due the phase noise.

2. LIPID STRUCTURES ADSORBED BY 5 MHZ CRYSTAL CHARACTERIZATION

The criteria to identify the absorption of the liposomes into the crystal and its transition to lipid bilayer is based on the Reviakine [35], Keller [32] and Erik [34] works and consists in:

- Increase and decrease in dissipation. The liposomes are absorbed causing an increase in dissipation, breaking afterwards and forming a bilayer. As the bilayer has an elastic behavior, the dissipation will return to the starting values.
- Convex form in frequency. The frequency decreases as the liposome adheres to the surface of the crystal. When a critical point of covering is achieved, the liposomes break forming a bilayer. Frequency will increase until reaching approximately -25 Hz, equivalent to the DOPC bilayer mass.

In figure 18, all 5 MHz experiments exposed in Table 14 and tagged as "Good" or "Ok" that follow the bilayer criteria are represented.
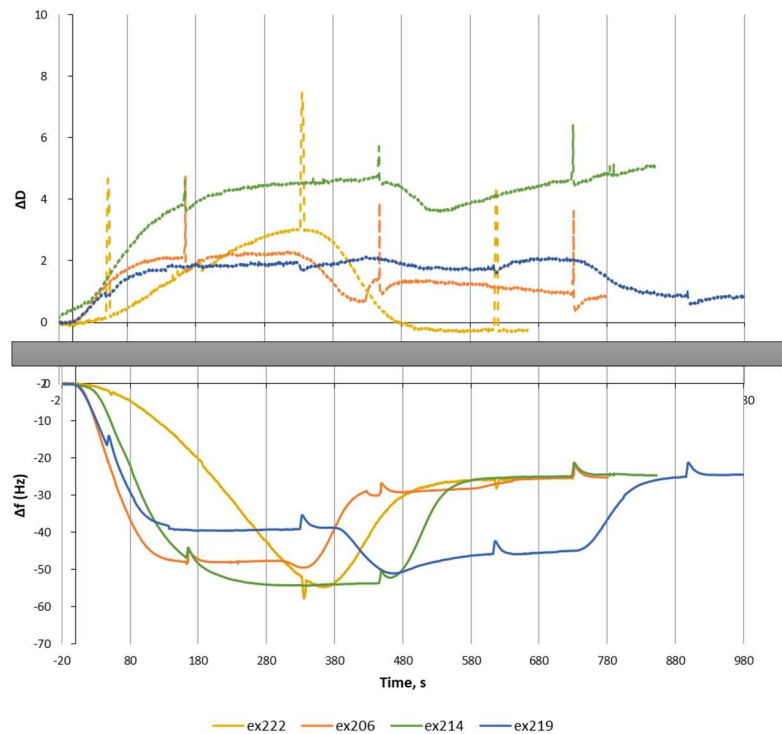
figure 18: Lipidic bilayer formation for 5MHz crystals. The experiments used are tagged as "Good" or
"Ok" quality.

In figure 18 we can see that all the experiments end at the same frequency of 25 Hz. Some dissipation curves didn't reach zero as expected. The explanation for this that some experiments present a drift in dissipation, this especially visible in experiment ex214 (green).

Other aspect to discuss is the irregular duration of the experiments. That is because it was necessary perform several injections of lipids, being able to cause a "pause" before reaching the critical point of covering and break into a lipid bilayer.

 In conclusion we find that we had successful lipid bilayers in the 5 MHz crystals.

3. LIPID STRUCTURES ADSORBED BY 100 MHZ CRYSTAL CHARACTERIZATION

Like in 5 MHz crystals, two possible lipid structures are expected in the 100 MHz crystals. In the first, the vesicles adhere to the crystal surface and break forming a surface bilayer or SB. In the second, the vesicles didn't break and remain attached forming a surface vesicular layer or SVL.

It is possible deduce 2 features that the surface bilayer absorption will have in 100 MHz crystal:

- The dissipation will grow up during liposome adsorption and then decrease and return to zero due liposome break and the bilayer formation.

- The final frequency shift will fulfil the Sauerbrey equation, in other words, the final frequency shit will be proportional to the mass of the bilayer adsorbed

64

If the assumptions are correct and a lipid bilayer form in the surface of the 100 MHz crystals, the mass of the bilayer adsorbed should be equal to the mass adsorbed by the 5 MHz crystal.

In figure 21, all 100 MHz experiments tagged as "Good" or "Ok" in the Table 14 that follow the bilayer criteria is represented.
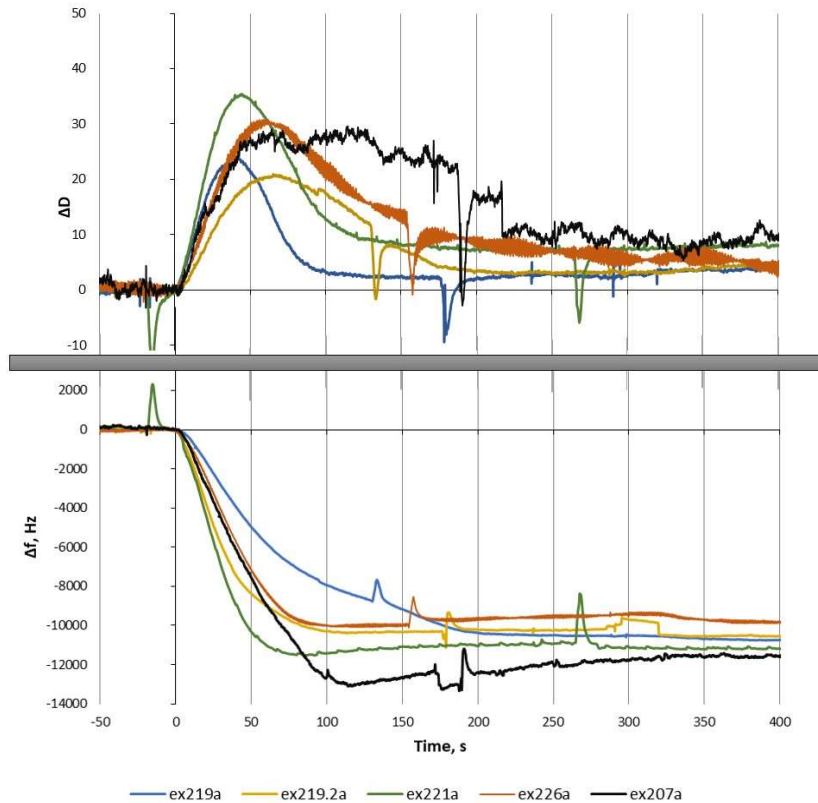
figure 21: Lipidic bilayer formation for 100MHz crystals. The experiments used are tagged as "Good" or "Ok" quality.

Analyzing the data obtained with comparing it with the standard shape of a liposome transition to a bilayer, figure 20, we extract the following conclusions:

- It is possible to see that the experiment "ex207a" (black) and the experiment "ex226a" are affected by noise, probably by small bubbles that affect the stability.

- There is no well-defined minimum in frequency like the one what can be seen in the 5 MHz experiments although in some of them it is slightly visible.

- Despite the decrease in dissipation that indicate the liposome breakdown, in no experiment the dissipation reaches a value of zero.

- All the process happens between 300 seconds and 350 seconds.

The reason that no experiment reached dissipation zero could be that the 100 MHz crystal is more sensitive to the viscoelastic properties of the bilayer[39]. This is because the bilayer is too thin for the classical sensors to perceive its viscoelastic properties as described in figure 7.

4. COMPARATION BETWEEN LIPOSOME ADSORPTION AND BILAYER ADSORPTION IN THE SURFACE OF 100 MHZ CRYSTAL.

Characterize liposome adsorption in 100 MHz crystals can be more difficult. Liposomes don't follow the Sauerbrey relation, for this reason a specific model should be used to characterize them. However, there is no need to characterize them quantitatively, it is possible recognize them only qualitatively.

In the following table the results tagged with the "Good" or "Ok" label are averaged.

100 MHz	Δf (Hz)	Mass (ng/cm2)	ΔD (*1E-6)	Max D (*1E-6)
Liposomes	-28802±4246	1221±184	144±24	149±29
Bilayer	-10619±580	447.5±24.9	6.01±2.78	28.3±5.70

The most important differences between the liposomes and the bilayer adsorption are:

- The final frequency: the liposomes cause a greater change in frequency

- Maximum in dissipation: the energy dissipated by the liposomes is bigger, even in the critical point of the bilayer adsorption.

- Dissipation tendency: the bilayer adsorption dissipation will return to zero eventually

- Slope of the frequency and the dissipation: the increase and decrease of dissipation and frequency, correspondingly, are bigger for the liposome adsorption.

- Time of stabilization: We find that the process of bilayer adsorption (100s) is faster than the liposome adsorption (230s).
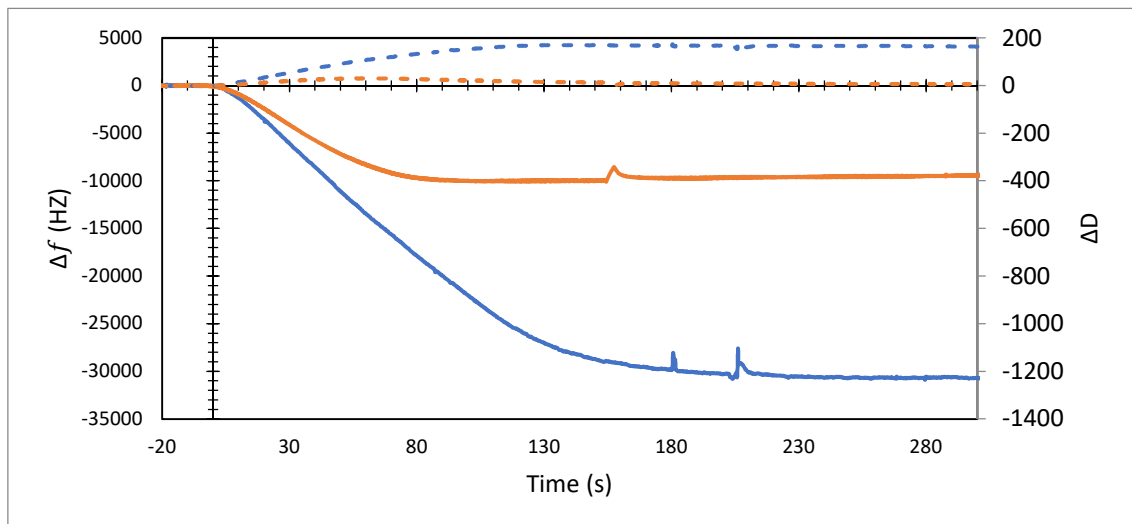
figure 22: Comparation between the experiment ex206b where liposomes are adsorbed (blue) and the experiment ex226b where a bilayer is formed (orange). The frequency change is represented with a continuous line and the dissipation change is represented with a discontinuous line.

5. COMPARATION BETWEEN THE MASS PERCIEVED BY A 100 MHZ CRYSTAL AND A 5 MHZ CRYSTAL

Finally, we compare the mass of the bilayer as determined with in the 100 MHz crystal with the mass adsorbed in the 5 MHz crystal using the Sauerbrey relation. Using the experiments that were as "Good" or "Ok" in terms of signal quality (as defined above), we calculated the mean and the standard deviation of the obtained mass and dissipation values.

Crystal	Δf (Hz)	Mass (ng/cm2)	ΔD (*1E-6)	Max D (*1E-6)
100 MHz	-10619±580	450±25	6.01±2.78	28.3±5.70
5 MHz	-24.62±0.91	420±16	0.62±0.56	2.53±0.63

To within the experimental error, the two sets of masses are very similar.

The differences founded between the adsorption of a bilayer in a 100 MHz crystal and a 5 MHz are:

Time of stabilization: We found that the process of bilayer formation is faster in the 100 MHz crystal (200s) than in the 5 MHz crystal (550s). The principal explanation is the reduced dimensions of the 100 MHz crystal surface.

A bigger sensitivity in dissipation for the 100 MHz crystal: We obtained a dissipation sensitivity 5 times bigger for the 100 MHz crystal. It is possible to speculate that the 100MHz crystal can bring more information about the lipid bilayer nanomechanics.

Maximum peak in mass of the 5 MHz crystal: the peak corresponding to the critical point of liposome adsorption is not visible in the 100 MHz crystal. One explanation could be that the reduced dimensions of the 100 MHz prevents the accumulation of liposomes and the critical point is produced before the totally of the surface of the crystal is covered.

The dissipation variation of the 100 MHz crystal experiments never returns completely to zero. The explanation could be that the HFF crystals are more sensitive to the viscoelastic properties of the lipid bilayer. In the case of the 5 MHz crystal the bilayer result to thin and the dissipation goes to zero
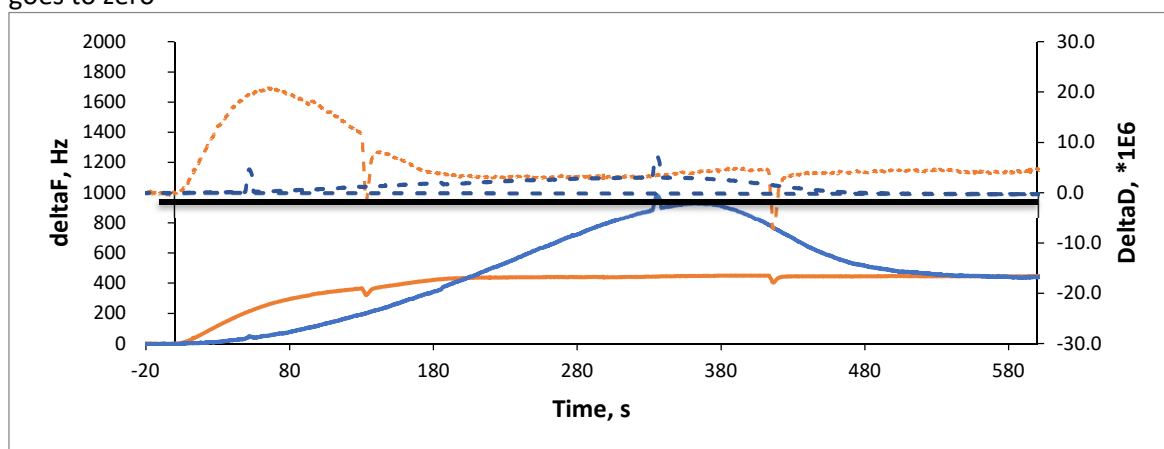
Figure 23: Comparation between the experiment ex222 where a 5 MHz crystal is used (blue) and the experiment ex226b where a 100MHz crystal is used (red). The mass change is represented with a continuous line and the dissipation change is represented with a discontinuous line.

Conclusion

Comparison of the performance of 100 MHz crystal and 5 MHz QCM crystals allowed us to conclude that:

1. It is possible to form a phospholipidic bilayer in a SiO2-coated HFF crystal: for the first time we were able to forma DOPC bilayer in a 100 MHz quartz crystal coated with SiO_2

2. The sensitivity of the HFF crystals is similar to the regular crystals: Instead of the expected increase in sensitivity of 400 for the 100 MHz crystal based on the Sauerbrey constant, we obtained sensitivity that is very similar to that of the 5 MHz crystal. This is surprising.

3. The 100 MHz crystals are less robust than the 5 MHz crystals and present more variation in sensitivity between different crystals.

4. In some 100 MHz crystal experiments, the vesicular layer didn't break. The most plausible explanation is a deficient cleaning or a bad SiO_2 coating in combination to the reduced dimensions of the crystal.

5. The reduced dimensions of the 100 MHz crystal cause the vesicular layer to break earlier than the 5 MHz crystals (figure 23). Consequently, there is a faster formation of the lipid bilayer and the breaking of the liposomes.

6. No peak in frequency shift is observed during the bilayer formation on the 100 MHz crystals. It is observed when the same experiment is done with the 5 MHz crystals.

7. The resolution in dissipation is 5 times bigger for the 100 MHz crystals than for the 5 MHz crystals. That means that the HFF crystals can obtain new nanomechanical information of the lipid bilayer. This will have a major consequence: The 100 MHz crystal is capable of sensing the viscoelastic properties of the lipid bilayer. In the case of the 5 MHz crystal, the bilayer is too thin, and the dissipation change produced is below its resolution (figure 23). This is particularly shocking because it means that the lipid bilayer dissipates more energy of the 100 MHz shear waves than the 5 MHz shear waves. As far as we understand, the discovery of this phenomenon is completely new and could have a great impact in the understanding of nanomechanical sensing with HFF crystals.

Initially, it seems that HFF crystals don't represent a breakthrough in terms of sensitivity, though that was the main reason of using crystals with a higher resonance frequency. However, the reduction of the area sensed and the increase in dissipation sensitivity are promising for biosensing applications and opens new possibilities for the acoustic wave sensing field.

Bibliography

1. Turner, A. P. F., Karube, I., Wilson, G. S. & Worsfold, P. J. Biosensors: fundamentals and applications. *Anal. Chim. Acta* **201,** 363–364 (1987).

2. Cammann, K. *et al.* Chemical Sensors and Biosensors—Principles and Applications. *Angew. Chemie Int. Ed. English* **30,** 516–539 (1991).

3. Sharma, S., Byrne, H. & O'Kennedy, R. J. Antibodies and antibody-derived analytical biosensors. *Essays Biochem.* **60,** 9–18 (2016).

4. Phadke, R. S. Biosensors and enzyme immobilized electrodes. *Biosystems* **27,** 203–206 (1992).

5. Rashid, J. I. A. & Yusof, N. A. The strategies of DNA immobilization and hybridization detection mechanism in the construction of electrochemical DNA sensor: A review. *Sens. Bio-Sensing Res.* **16,** 19–31 (2017).

6. Gui, Q., Lawson, T., Shan, S., Yan, L. & Liu, Y. The Application of Whole Cell-Based Biosensors for Use in Environmental Analysis and in Medical Diagnostics. *Sensors (Basel).* **17,** (2017).

7. Bhalla, N., Jolly, P., Formisano, N. & Estrela, P. Introduction to biosensors. *Essays Biochem.* **60,** 1–8 (2016).

8. Tellechea, E., Johannsmann, D., Steinmetz, N. F., Richter, R. P. & Reviakine, I. Model-Independent Analysis of QCM Data on Colloidal Particle Adsorption. *Langmuir* **25,** 5177–5184 (2009).

9. Sauerbrey, G. Verwendung von Schwingquarzen zur W�gung d�nner Schichten und zur Mikrow�gung. *Zeitschrift f�r Phys.* **155,** 206–222 (1959).

10. Walls, F. L. & Vig, J. R. Fundamental Limits on the Frequency Stabilities of Crystal Oscillators. *IEEE Trans. Ultrason. Ferroelectr. Freq. Control* **42,** 576–589 (1995).

11. Ballato, A. & Gualtieri, J. G. Advances in high-Q piezoelectric resonator materials and devices. *IEEE Trans. Ultrason. Ferroelectr. Freq. Control* **41,** 834–844 (1994).

12. Palasantzas, G. Quality factor due to roughness scattering of shear horizontal surface acoustic waves in nanoresonators. *J. Appl. Phys.* **104,** 053524 (2008).

13. Arnau, A., Montagut, Y., García, J. V. & Jiménez, Y. A different point of view on the sensitivity of quartz crystal microbalance sensors. *Meas. Sci. Technol.* **20,** (2009).

14. Oswald, P. *Rheophysics : the deformation and flow of matter*. (Cambridge University Press, 2009).

15. Ferry, J. D. *Viscoelastic properties of polymers*. (Wiley, 1980).

16. Sagmeister, B. P., Graz, I. M., Schwödiauer, R., Gruber, H. & Bauer, S. User-friendly, miniature biosensor flow cell for fragile high fundamental frequency quartz crystal resonators. *Biosens. Bioelectron.* **24,** 2643–2648 (2009).

17. Fernández, R. *et al.* Design and validation of a 150 MHz HFFQCM sensor for bio-sensing applications. *Sensors (Switzerland)* **17,** 1–13 (2017).

18. Zimmermann, B., Lucklum, R., Hauptmann, P., Rabe, J. & Büttgenbach, S. Electrical characterisation of high-frequency thickness-shear-mode resonators by impedance analysis. *Sensors Actuators, B Chem.* **76,** 47–57 (2001).

19. Vig, J. R. & Walls, F. L. A review of sensor sensitivity and stability. *Proc. Annu. IEEE Int. Freq. Control Symp.* 30–33 (2000). doi:10.1109/FREQ.2000.887325

20. Lec, R. M. Piezoelectric biosensors: recent advances and applications. in *Proceedings of the 2001 IEEE International Frequncy Control Symposium and PDA Exhibition (Cat. No.01CH37218)* 419–429 (IEEE). doi:10.1109/FREQ.2001.956265

21. Rabe, J., Buttgenbach, S., Zimmermann, B. & Hauptmann, P. Design, manufacturing, and characterization of high-frequency thickness-shear mode resonators. in *Proceedings of the 2000 IEEE/EIA International Frequency Control Symposium and Exhibition (Cat. No.00CH37052)* 106–112 (IEEE). doi:10.1109/FREQ.2000.887338

22. Uttenthaler, E., Schräml, M., Mandel, J. & Drost, S. Ultrasensitive quartz crystal microbalance sensors for detection of M13-Phages in liquids. *Biosens. Bioelectron.* **16,** 735–743 (2001).

23. Vig, J. R. & Meeker, T. R. The aging of bulk acoustic wave resonators, filters and oscillators. *Proc. 45th Annu. Symp. Freq. Control 1991* 77–101 (1991). doi:10.1109/FREQ.1991.145888

24. Shockley, W., Curran, D. R. & Koneval, D. J. Energy Trapping and Related Studies of Multiple Electrode Filter Crystals. *17th Annu. Symp. Freq. Control* **7,** 88–126 (1963).

25. March, C. *et al.* High-frequency phase shift measurement greatly enhances the sensitivity of QCM immunosensors. *Biosens. Bioelectron.* **65,** 1–8 (2015).

26. Cervera-Chiner, L. *et al.* High Fundamental Frequency Quartz Crystal Microbalance (HFF-QCM) immunosensor for pesticide detection in honey. *Food Control* **92,** 1–6 (2018).

27. Montagut, Y. *et al.* QCM Technology in Biosensors. in *Biosensors - Emerging Materials and Applications* (InTech, 2011). doi:10.5772/17991

28. Richter, R. P., Bérat, R. & Brisson, A. R. Formation of solid-supported lipid bilayers: An integrated view. *Langmuir* **22,** 3497–3505 (2006).

29. Castellana, E. T. & Cremer, P. S. Solid supported lipid bilayers: From biophysical studies to sensor design. *Surf. Sci. Rep.* **61,** 429–444 (2006).

30. Kanásová, M. & Nesměrák, K. Systematic review of liposomes' characterization methods. *Monatshefte für Chemie - Chem. Mon.* **148,** (1994).

31. Attwood, S. J., Choi, Y. & Leonenko, Z. Preparation of DOPC and DPPC supported planar

lipid bilayers for atomic force microscopy and atomic force spectroscopy. *Int. J. Mol. Sci.* **14,** 3514–3539 (2013).

32. Keller, C. A. & Kasemo, B. Surface specific kinetics of lipid vesicle adsorption measured with a quartz crystal microbalance. *Biophys. J.* **75,** 1397–1402 (1998).

33. Voinova, M. V., Jonson, M. & Kasemo, B. 'Missing mass' effect in biosensor's QCM applications. *Biosens. Bioelectron.* **17,** 835–841 (2002).

34. Erik Reimhult, *, Fredrik Höök, and & Kasemo, B. Intact Vesicle Adsorption and Supported Biomembrane Formation from Vesicles in Solution: Influence of Surface Chemistry, Vesicle Size, Temperature, and Osmotic Pressure†. (2002). doi:10.1021/LA0263920

35. Reviakine, I., Johannsmann, D. & Richter, R. P. Hearing what you cannot see and visualizing what you hear: Interpreting quartz crystal microbalance data from solvated interfaces. *Anal. Chem.* **83,** 8838–8848 (2011).

36. and, I. R. & Brisson*, A. Formation of Supported Phospholipid Bilayers from Unilamellar Vesicles Investigated by Atomic Force Microscopy. (2000). doi:10.1021/LA9903043

37. Höök, F. *et al.* A comparative study of protein adsorption on titanium oxide surfaces using in situ ellipsometry, optical waveguide lightmode spectroscopy, and quartz crystal microbalance/dissipation. *Colloids Surfaces B Biointerfaces* **24,** 155–170 (2002).

38. Cao-Paz, A. M., Rodríguez-Pardo, L., Fariña, J. & Marcos-Acevedo, J. Resolution in QCM sensors for the viscosity and density of liquids: Application to lead acid batteries. *Sensors (Switzerland)* **12,** 10604–10620 (2012).

39. Reviakine, I., Simon, A. & Brisson, A. Effect of Ca $^{2+}$ on the Morphology of Mixed DPPC–DOPS Supported Phospholipid Bilayers. *Langmuir* **16,** 1473–1477 (2000).

DOCUMENT 2:

BUDGET

Budget Index

Budget introduction

This document studies the budget of the Thesis to determinate the economic viability through the calculation of the investment that the project would require. This economic study divides de experimental procedures in chapters. Then, the materials, machinery and workforce of every chapter was budgeted. From this data the decomposed price chart by chapter was determined and next, the partial budget of each chapter.

Finally, the budget for the execution of the materials, the budget execution by contract and the general project budget was calculated.

The resources used were classified using a code according to their nature. The description of the codes used is summarized in the next table.

Table 15: Different used resource categories in the budged.

Code	Description
LM	lab material
CH	chemical reactive
EM	experimentation material
MC	machinery

1. MATERIALS CHART

The next table shows all the materials used during the realization of this Thesis

Nº	Reference	Unit	Description	Amount		
				Quantity	Cost (€)	Total (€)
Chemical reactives						
1	CH.1	G	DOPC >99% (TLC) Avanti	0.05	50	2.5
2	CH.2	G	HEPES ≥99.5% (titration)	15	0.75	11.25
3	CH.3	G	NaCl	15	0.3	4.5
4	CH.4	G	$CaCl_2$	50	0.4	20
5	CH.5	L	NaOH	0.05	30	1.5
6	CH.6	L	Chloroform	0.4	7	2.8
7	CH.7	L	Nano pure water Panreac	100.3	8	802.4
8	CH.8	L	Ethanol Panreac	5.1	8	40.8
9	CH.9	L	SDS	0.85	3.2	2.72
10	CH.10	Ud	Nitrogen bottle	2	67	134
				Amount		**1022.47**

Nº	Reference	Unit	Description	Quantity	Cost (€)	Total (€)
Exmerimentation materials						
11	EM.1	ud	AWS 5 MHz quartz crystal coated with SiO2	34	0.82	27.88
12	EM.2	ud	AWS 100 MHz quartz crystal coated with SiO2	34	1.24	42.16
13	LM.1	ud	AWS QCM cell (5 MHz crystal)	34	0.25	8.5
14	LM.2	ud	AWS QCM cell (5 MHz crystal)	34	0.4	13.6
					Amount	**92.14**

Nº	Reference	Unit	Description	Quantity	Cost (€)	Total (€)
Lab equipment						
15	LM.3	ud	Protection glasses	1	13	13
16	LM.4	ud	Latex glove box	1	7.5	7.5
17	LM.5	ud	Lab coat		17	0
18	LM.6	ud	Paper roll	3	4	12
19	LM.7	ud	micropipette tip box	1	46	46
20	LM.8	ud	Micropipette 150 µL	1	230	230
21	LM.9	ud	Micropipette 1000 µL	1	145	145
22	LM.10	ud	Metallic spoon	1	4	4
23	LM.11	ud	centrifuge tube	3	6	18
24	LM.12	ud	Beaker 250ml	3	7	21
25	LM.13	ud	ISO flask 1L	2	14	28
26	LM.14	ud	spatula	1	3	3
27	LM.15	ud	nitrile glove box	1	12	12
28	LM.16	ud	stirring magnet	1	7.2	7.2
29	LM.17	ud	weighing paper	20	0.01	0.2
30	LM.18	ud	50ml glass beaker	3	6.4	19.2
31	LM.19	ud	Tweezers	2	19	38
32	LM.20	ud	Hamilton microliter syringe	1	29	29
33	LM.21	ud	Pasteur pipette	1	29	29
34	LM.22	ud	Cell culture dish	4	2	8
35	LM.23	ud	Plastic sirynge	34	0.4	13.6
36	LM.24	ud	test tube	34	0.75	25.5
37	LM.25	ud	syringe filter whatman	4	14.2	56.8
38	LM.26	ud	Plastic pipe	9	18	162
39	LM.27	ud	Eppendorf tube	34	0.2	6.8
40	LM.28	ud	graduated cylinder	1	13	13
					Amount	**947.8**
			Total amount (€)			**2062.41**

2. MACHINERY CHART

The amortization of the machinery used was calculated with the following equation.

$$P = \frac{Cost * t_{use}}{Per_{amort}}$$

The cost of using the machinery (P) is equal to the cost of the machine ($Cost$) multiplied by the time of use during the 5 months of experimentation (t_{use}) divided by the time of amortization (Per_{amort}). The amortization time selected was ten years.

The next table shows the costs of the machinery used in this Thesis.

Table 16: Machinery

Nº	Reference	Unit	Description	Amount		
				Cost (€)	quantity	Total (€)
1	MC.01	h	Q Sonica Q500 Sonicator	4	10	40
2	MC.02	h	5418R centrifuge refrigerated model	0.25	2	0.5
3	MC.03	h	Hanna EDGE pH/OD/EC	0.32	1	0.32
4	MC.04	h	Kern AES-C/AEJ-CM balance	0.2	1	0.2
5	MC.05	h	AWS F20 Research platform	6.3	68	428.4
6	MC.06	h	AWS A20 Research platform	5.2	68	353.6
7	MC.07	h	Network analyzer Agilent E5100A	6	3.52	21.12
8	MC.08	h	Zetasizer Nano ZS, Malvern	12	4	48
9	MC.09	h	EDA in-flow conductivity measurement monitor	8	34	272
10	MC.10	h	UV Ozone Cleaner – ProCleaner	25.5	0.83	21.165
			Total amount (€)			**1185.305**

3. WORKFORCE CHART

The workforce chart is described in the next table.

Table 17: Workforce chart

Nº	Reference	Unit	Description	Amount		
				Cost (€)	Quantity (h)	Total (€)
1	WF.01	h	Biomedical engineering student	3.75	300	1125
2	WF.02	h	Thesis' supervisor	25	74	1850
3	WF.03	h	Thesis' cosupervisor	25	16	400
			Total amount (€)			**3375**

4. DECOMPOSED PRICE

For the realization of the partial budged, all the experimental activities realized were divided in chapters and subchapters. This chapters correspond to the methods described in the "materials and methods sections with the addition of the meetings with the tutor and co-tutor. For every activity, the necessary materials, machinery and workforce is listed, and their total cost calculated for a single execution of this activity

Table 18: Decomposed price

Nº Reference	Chapter description				
	1. 10mM HEPES buffer preparation (1L)				
1.1	**Name**	**Quantity**	**Unit**	**Cost (€/u)**	**Partial Cost (€)**	**Total Cost (€)**
	Biomedical engineering master student	2	h	3.75	7.5	
	HEPES ≥99.5% (titration)	3	g	0.75	2.25	
	weighing paper	4	ud	0.01	0.04	
	NaCl	3	g	0.3	0.9	
	CaCl$_2$	10	g	0.4	4	
	NaOH	0.01	L	30	0.3	
	Nano pure water Panreac	1	L	8	8	
	Hanna EDGE pH/OD/EC	0.2	h	0.32	0.064	
	Kern AES-C/AEJ-CM balance	0.2	h	0.05	0.01	
	test tube	1	ud	0.75	0.75	
	auxiliary media	3	%	36	1.08	
	Indirect cost	3	%	42	1.26	
						26.2
	2. DOPC liposome preparation				
2.1	**Liposome synthesis**	**Quantity**	**Unit**	**Cost (€/u)**	**Partial Cost (€)**	**Total Cost (€)**
	Biomedical engineering master student	6	h	3.75	22.5	
	Thesis' supervisor	6	h	25	150	
	10mM HEPES buffer	1	L	26.154	26.154	
	DOPC >99% (TLC) Avanti	0.025	g	50	1.25	
	Chloroform	0.2	L	7	1.4	
	Nano pure water Panreac	0.5	L	8	4	
	Ultra pure argon	3	L	12	36	
	Q Sonica Q500 Sonicator	2	h	10	20	
	5418R centrifuge refrigerated model	1	h	0.25	0.25	
	centrifuge tube	3	ud	6	18	
	auxiliary media	3	%	242	7.26	
	Indirect cost	3	%	187	5.61	
						292.4

2.2	Name	Quantity	Unit	Cost (€/u)	Partial Cost (€)	Total Cost (€)
	Biomedical engineering master student	2	h	3.75	7.5	
	Thesis' supervisor	2	h	25	50	
	Zetasizer Nano ZS	2	h	12	24	
	auxiliary media	3	%	70	2.1	
	Indirect cost	3	%	93	2.79	
						86.4
	3. Experimentation procedure					
3.1	**Name**	**Quantity**	**Unit**	**Cost (€/u)**	**Partial Cost (€)**	**Total Cost (€)**
	Biomedical engineering master student	5	h	3.75	18.75	
	Thesis' supervisor	1	h	25	25	
	10mM HEPES buffer	0.1	L	26.154	2.6154	
	Ethanol Panreac	0.3	L	8	2.4	
	Nano Pure Water	0.5	L	8	4	
	SDS	0.05	L	3.2	0.16	
	EDA in-flow conductivity measurement monitor	2	h	8	16	
	AWS 5 MHz quartz crystal coated with SiO2	2	h	0.82	1.64	
	AWS 100 MHz quartz crystal coated with SiO2	2	h	1.24	2.48	
	AWS QCM cell (5 MHz crystal)	2	h	0.25	0.5	
	AWS QCM cell (100 MHz crystal)	2	h	0.4	0.8	
	AWS F20 Research platform	4	h	6.3	25.2	
	AWS A20 Research platform	4	h	5.2	20.8	
	UV Ozone Cleaner – ProCleaner	1.5	h	0.83	1.245	
	test tube	2	ud	0.75	1.5	
	Plastic sirynge	2	ud	0.4	0.8	
	Eppendorf tube	2	ud	0.2	0.4	
	auxiliary media	3	%	84	2.52	
	Indirect cost	3	%	63	1.89	
						128.7
	4. Inventoriable material					
4.1	**Name**	**Quantity**	**Unit**	**Cost (€/u)**	**Partial Cost (€)**	**Total Cost (€)**
	micropipette tip box	1	ud	46	46	
	Micropipette 150 µL	1	ud	230	230	
	Micropipette 1000 µL	1	ud	145	145	
	Beaker 250ml	3	ud	7	21	
	Sirynge filter	4	ud	14.2	56.8	
	ISO flask 1L	2	ud	14	28	
	stirring magnet	1	ud	7.2	7.2	
	50ml glass beaker	3	ud	6.4	19.2	

		Quantity	Unit	Cost (€/u)	Partial Cost (€)	Total Cost (€)
	Plastic pipe	9	ud	18	162	
	Paper roll	3	ud	4	12	
	Tweezers	2	ud	19	38	
	Metallic spoon	1	ud	4	4	
	spatula	1	ud	3	3	
	stirring magnet	1	ud	12	12	
	Nitrogen bottles	2	ud	68	136	
	Graduated cylinder	1	ud	13	13	
	Dewar flask	1	ud	36	36	
	Hamilton microliter syringe	1	ud	29	29	
	Pasteur pipette	1	ud	28	28	
	Network analyzer Agilent E5100A	6	h	3.52	21.12	
	Cell culture dish	4	ud	2	8	
						1055.3
5. Meetings						
5.1	**Planning and management meetings**	Quantity	Unit	Cost (€/u)	Partial Cost (€)	Total Cost (€)
	Biomedical engineering master student	2	h	3.75	7.5	
	Thesis' supervisor	1.5	h	25	37.5	
	auxiliary media	3	%	16	0.48	
	Indirect cost	3	%	10	0.3	
						45.78
5.2	**monitoring and control meetings**	Quantity	Unit	Cost (€/u)	Partial Cost (€)	Total Cost (€)
	Biomedical engineering master student	3	h	3.75	11.25	
	Thesis' supervisor	1.5	h	25	37.5	
	Thesis' cosupervisor	1.5	h	25	37.5	
	auxiliary media	3	%	14	0.42	
	Indirect cost	3	%	19	0.57	
						87.2
5.3	**Revisions and corrections**	Quantity	Unit	Cost (€/u)	Partial Cost (€)	Total Cost (€)
	Biomedical engineering master student	50	h	3.75	187.5	
	Thesis' supervisor	20	h	25	500	
	Thesis' cosupervisor	8	h	25	200	
	auxiliary media	3	%	33	0.99	
	Indirect cost	3	%	27	0.81	
						889.3

6. Individual protection and security						
6.1	**Name**	**Quantity**	**Unit**	**Cost (€/u)**	**Partial Cost (€)**	**Total Cost (€)**
	Protection glasses	1	ud	13	13	
	Latex glove box	1	ud	7.5	7.5	
	Lab coat	1	ud	17	17	
	Nitrile glove box	1	ud	12	12	
						49.5

5. PARTIAL BUDGET

The next table shows the partial budget for each chapter.

Table 19: Partial budget

Nº code	Chapter description				
1	**1. 10mM HEPES buffer preparation**				
	Description	**UD**	**Measurement**	**Cost (€)**	**Total cost (€)**
1.1	Buffer preparation	ud	5	26.154	
	Partial budget chapter 1				**130.77**
2	**2. DOPC liposome preparation**				
	Description	**UD**	**Measurement**	**Cost (€)**	**Total cost (€)**
2.1	Liposome syntesis	ud	2	292.424	
2.2	Liposome characterization	ud	2	86.39	
	Partial budget chapter 2				**757.63**
3	**3. Experimentation procedure**				
	Description	**UD**	**Measurement**	**Cost (€)**	**Total cost (€)**
3.1	Experimental setup	ud	17	128.7004	
	Partial budget chapter 3				**2187.91**
4	**4. Inventoriable material**				
	Description	**UD**	**Measurement**	**Cost (€)**	**Total cost (€)**
4.1	Inventoriable material	ud	1	1055.32	
	Partial budget chapter 4				**1055.32**
5	**5. Meetings**				
	Description	**UD**	**Measurement**	**Cost (€)**	**Total cost (€)**
5.1	Planning and management meetings	ud	8	45.78	
5.2	monitoring and control meetings	ud	6	87.24	
5.3	Revisions and corrections	ud	1	889.3	
	Partial budget chapter 5				**1778.98**
6	**6. Individual protection and security**				
	Description	**UD**	**Measurement**	**Cost (€)**	**Total cost (€)**
6.1	Individual protection and security	ud	1	49.5	
	Partial budget chapter 6				**49.5**

6. MATERIAL EXECUTION BUDGET, EXECUTION BY CONTRACT BUDGET AND GENERAL PROJECT BUDGET

The material execution budget is the sum of the partial budgets. The execution by contract budget was calculated as the sum of the material execution budget and the general costs applicable to this budget (13% of the material execution budget). At least, to obtain the general project budget the IVA (21%) was applied to the execution by contract budget.

material execution budget, execution by contract budget and general project budget

1. 10mM HEPES buffer preparation	130.77
2. DOPC liposome preparation	757.628
3. Experimentation procedure	2187.90
4. Inventoriable material	1055.32
5. Meetings	1778.98
6. Individual protection and security	49.5
Total: ………….	5960.10 €

The material execution budget goes up to the quantity of FIVE THOUSAND NINE HANDRED SIXY POINT TEN EUROS.

Material execution budget	5960.10 €
General expenses 13%	774.81
Industrial benefit	0
Budget execution by contract	6734.92 €

The execution by contract budget goes up to the quantity of SIX THOUSAND SEVEN HANDRED THIRTY-FOUR POINT NINETY-TWO EUROS.

Budget execution by contract	5960.10
IVA 21%	1251.62
General project budget	7211.72

The General project budget goes up to the quantity of SEVEN THOUSAND TOW HANDRED ELEVEN POINT SEVENTY-TWO EUROS.